THE UNIVERSITY OF CHICAGO

STRUCTURE OF CRUMPLED THIN ELASTIC MEMBRANES

A DISSERTATION SUBMITTED TO

THE FACULTY OF THE DIVISION OF PHYSICAL SCIENCES

IN CANDIDACY FOR THE DEGREE OF

DOCTOR OF PHILOSOPHY

DEPARTMENT OF PHYSICS

BY

ALEXANDER E. LOBKOVSKY

CHICAGO, ILLINOIS

AUGUST, 1996

ACKNOWLEDGMENTS

I am indebted to a number of people in the physics department at the University of Chicago for greatly enhancing my graduate school experience. Extensive discussions with my advisor, Professor Thomas A. Witten taught me how to think like a physicist and were an inexhaustible source of fruitful ideas. His careful and persistent interest in my progress served as a constant motivation to learn and achieve. Much of the work presented here was done in collaboration with Eric M. Kramer, with whom I had numerous eye opening and enjoyable discussions. I am grateful to Thomas C. Halsey for being my mentor during the critical second year at the University of Chicago. I am extremely fortunate to have had the opportunity to collaborate with Hao Li, from whom I learned a tremendous amount. Eli Ben-Naim provided help and wisdom that proved invaluable to my formation as a physicist. My sincere and warm thanks go to all of my friends, whose support and encouragement made the graduate school bearable. I would like to thank Professors David Greer, Robert Geroch and Emil Martinec, for agreeing to serve on my thesis committee.

Finally, I would like to dedicate this thesis to the people who really made it possible: my parents who supported and encouraged my venture into the world of science in my early years and who continue to give me their love and affirmation; and Laura J. Pinnas, whose love, support and advice sustain and reinvigorate my existence and have helped me through the thick and thin of my tenure at Chicago.

TABLE OF CONTENTS

LIST OF ILLUSTRATIONS

ABSTRACT

In this thesis we explore forced crumpling of a thin elastic membrane. As in many problems that involve bending of elastic plates and shells, the limit of the vanishing membrane thickness leads to a boundary layer phenomenon. We argue that the structure of a crumpled sheet in that limit is simple. It consists of a collection of flat facets that are bounded by straight edges that in turn meet at sharp vertices. These edges become infinitely sharp in the small thickness limit. A boundary layer solution in the ridge region determines the details of how the singular limit of a sharp crease is approached. Most of the elastic energy is confined into the ridges. A scaling law allows one to estimate the energy of a ridge given only its length and dihedral angle. Thus, if for a given compression factor, a crumpled sheet can be characterized in terms of the underlying ridge network, on can estimate its elastic energy and therefore its resistance to further compression.

CHAPTER 1

INTRODUCTION

Mechanical properties of thin elastic membranes are of great scientific and practical importance. Systems that can be described in the framework of membrane elasticity span a wide range of scales. Post-buckling properties of macroscopic plates and shells are important in engineering of thin-walled structures. Behavior immediately following a structural failure is relevant to safety engineering [1]. Understanding of the mechanical properties of collapsed or crumpled sheets can be useful in designing materials with favorable cushioning properties [2].

On the microscopic scale, many biological lipid-bilayer membranes behave as elastic plates if the lipid bilayer is reinforced somehow to resist shear deformations. The cyto-skeleton of a red blood cell membrane serves such a purpose [3]. *In vitro* lipid bilayers behave as solid membranes below the two dimensional (2D) freezing point or when polymerized [4]. Mechanical properties of these lipid membranes may be important in understanding such processes as passage of red blood cells through capillaries, cell division and usage of lipid vesicles for drug delivery [5].

Some inorganic compounds appear in the of form large monomolecular sheets that behave elastically on length scales large compared to interatomic spacing. Examples include molybdenum disulphite [6] and graphite oxide [7]. The conformation of these membranes in solution can be manipulated by changing such properties of the solvent. Changing the pH of the solution influences the van der Vaals attraction of the distant parts of the sheets and thus leads to a transition from a crumpled to a flat phase.

Mechanical and statistical properties of elastic membranes are a subject of great current interest [8]. Several types of distortion have been recently analyzed. Linear stability and the onset of buckling of thin-walled structures is understood in

great detail. For an exhaustive work on buckling of cylindrical shells see for example Yamaki [9]. Thermal fluctuations roughen the membrane but do not destroy its flatness, *i.e.* the normal-normal correlation function approaches a constant at large separations. If certain defects are introduced into the membrane via the boundary, it looses its global flatness [10]. Energy associated with such defects is well understood [11].

A separate class of problems that involve deformations of thin elastic membranes focuses on obtaining general results about behavior of shells in the small thickness limit. This particular question has no counterpart in problems that involve deformation of bulk objects. Several specific weak distortions of thin plates and shells have been analyzed in terms of their behavior in the limit of the vanishing shell thickness [12, 13, 14]. A common feature that emerges from these studies is that boundary layers of different flavors arise in a wide variety of situations. Membrane stresses are confined to these boundary layers whose width vanishes as some power of the shell thickness. We are interested in a complimentary regime of strong distortion of a membrane that is collapsed, or crumpled by external forces. We would like to establish the details of the structure of a crumpled membrane. In particular, formation of boundary layers in the limit of small thickness is anticipated. Scaling properties of these singularities must be understood and contrasted with other types of boundary layers in bending of thin plates and shells. Once the formation of the boundary layers is understood, one is able to make far-reaching predictions of the structure and the mechanical properties of a crumpled membrane since the distortions are confined to boundary layers in which the scaling properties of the elastic stresses are known.

It is important to understand the origin of such confinement. A variety of problems in other fields of physics exhibit similar confinement. There are several different types of situations. On the one hand, when some systems are strongly perturbed so that their linear response properties no longer describe their behavior, the perturbing energy is sometimes focused or confined to a small subset of the system. Examples include dielectric breakdown [15], crack formation in brittle fracture [16], formation of fibrils in stretching [17] and cracking of polymers [18], magnetic flux

vortices in type II superconductors [19], or pattern formation in hydrodynamic flows, solidification dynamics, and biological systems [20]. In other systems, a certain field is confined to a small subset of the available configuration space even in the ground or metastable state of the system. Examples include the Prandtl's boundary layer in high Reynolds number flows [21], organization of defects into grain boundaries in polycrystalline materials [22], rare-earth dopant distribution in creep-resistant alumina ceramics [23], force chains in granular packs [24], confinement of color gauge fields in quantum chromo-dynamics [25], or compactification of space dimensions in superstring theories [26].

In Chapter one of the thesis, we trace the development of the equations that describe large deflections of thin plates and give a simple derivation of the von Kármán equations of a plate. A review of various boundary layer phenomena that arise in bending of thin plates and shells is presented. In some of these phenomena the shell equations break down in some region of the distorted shell so that the full three dimensional elasticity equations must be used to properly capture the behavior of the shell in that region. One then must determine the correct effective boundary conditions for the rest of the shell. We are not interested in boundary layers of that sort since they are highly dependent on the details of the deformation. In other cases, however, the two dimensional (2D) plate or shell equations can, in fact, properly account for the rapid change of the stresses in the boundary layer. In that case, a boundary layer analysis of the thin shell equations produces the asymptotic scaling properties of the boundary layer in the limit of the vanishing shell thickness. We argue in the concluding section of Chapter 2 that a crumpled sheet exhibits boundary layers of the two types. First, there are sharp points of high curvature that must be described within the full three dimensional elasticity since the strains in these regions are of order unity. Second, these sharp points are connected by straight sharp ridges whose properties can, in fact, be accounted for by the von Kármán plate equations.

In the third Chapter we present the boundary layer analysis of the straight ridge singularity within a simple strip geometry. Singular boundary conditions are required in order for the ridge singularity to develop. A number of the scaling proper-

ties of the ridge turn out to be independent of the details of the boundary conditions. They are a function of a few geometric attributes of the ridge such as its length and dihedral angle. These include the scaling of the characteristic ridge width with the thickness of the plate and with the dihedral angle of the ridge. The shape of the ridge midline is also independent of the detail of the boundary conditions once the vertical displacement of the center of the ridge is specified. Other asymptotic properties of the ridge singularity such as the transverse ridge shape and the coefficients in the thickness scaling laws are dependent on the detailed form of the boundary conditions, such as the externally imposed compressive stress, for example.

CHAPTER 2

THIN SHELL EQUATIONS AND BOUNDARY LAYER PHENOMENA

2.1. Derivation of the von Kármán Plate Equations

Despite the fact that equations describing large deflections of thin plates were written down by Föppl in 1907 [27] and put on a firmer ground by von Kármán [28] three years later, much analytical work has been done since [29, 30, 31] to establish the degree of their accuracy and clarify limits of their applicability. Deformation of a bulk three dimensional body is described fully by a rank two symmetric stress tensor that is a function of the material coordinates. Thin shell equations are obtained in an attempt to reduce the number spatial variables in the problem by introducing moments of the stress tensor with respect to the integration over the shell thickness. The hope is that one can keep only a small number of these moments since higher moments will be of higher order in some small expansion parameter because the stresses do not vary significantly throughout the thickness of the shell. Rigorous analyses of this sort performed in various contexts can be found for example in Refs. [29] and [31].

These analyses indicate that when the strains are small and the radii of curvature of the middle surface are large compared to the thickness of the plate, first, the shell can be treated as a two dimensional object; and second, there is a hierarchy of equations for the moments of the stress tensor. Each successive level in that hierarchy is of higher order in some small parameter that has to be defined in each situation separately. In our case this parameter is the upper bound on the strain in the sheet. At zeroth order one obtains the well-known von Kármán equations for large deflections of thin plates. Here we reproduce a less rigorous derivation of these equations. Our derivation closely follows that of Ref. [32] with the exception of the

way in which we introduce the curvature potential f. We will point out the conditions that are necessary and sufficient in many practical situations to ensure the validity of the von Kármán equations. Note that this derivation can be generalized to describe shells that have a preferred curvature in the unstressed state. For a derivation see for example Ref. [33].

The two von Kármán equations have different origins. Let us begin with the derivation of the von Kármán equation that has a purely geometric origin. Let the points in the middle surface of the plate be labeled by x_α with $\alpha = 1, 2$. Then, the three dimensional conformation of the distorted membrane is given by $\vec{\mathbf{r}}(x_\alpha) \in \mathbf{R}^3$. The first and second fundamental forms better known as the metric tensor $g_{\alpha\beta}$ and the curvature tensor $C_{\alpha\beta}$ given by

$$g_{\alpha\beta} = (\partial_\alpha \vec{\mathbf{r}}) \cdot (\partial_\beta \vec{\mathbf{r}}) \tag{2.1}$$

$$C_{\alpha\beta} = \hat{\mathbf{n}} \cdot (\partial_\alpha \partial_\beta \vec{\mathbf{r}}), \tag{2.2}$$

are the objects that are closely related to the stresses in the shell. To clarify the meaning of these tensors we first note that the strain tensor $\gamma_{\alpha\beta}$ is defined as the deviation of the metric tensor from the identity

$$g_{\alpha\beta} = \delta_{\alpha\beta} + 2\gamma_{\alpha\beta}. \tag{2.3}$$

The sum of the eigenvalues of the strain tensor $\gamma_1 + \gamma_2$ is the (2D) expansion (or compression) factor and their difference is the shear angle [34]. The eigenvalues of the curvature tensor C_1 and C_2, on the other hand, are the inverses of the two principal radii of curvature of the surface. To be absolutely rigorous one must distinguish upper and lower indices, but since we define all quantities to first nontrivial order in the strain $\gamma_{\alpha\beta}$ and raising and lowering of the indices is accomplished by applying the metric tensor $g_{\alpha\beta}$, raising and lowering indices only affects higher order terms in $\gamma_{\alpha\beta}$.

In order for the tensors $g_{\alpha\beta}$ and $C_{\alpha\beta}$ to define a surface they must satisfy two relations involving the Christoffel symbols $\Gamma_{\alpha\beta\mu}$ [35] which are defined in terms of the metric tensor. When the strains are small the expression is particularly simple:

$$\Gamma_{\alpha\beta\mu} = -\partial_\mu \gamma_{\alpha\beta} + \partial_\alpha \gamma_{\beta\mu} + \partial_\beta \gamma_{\alpha\mu}. \tag{2.4}$$

The first relation which $g_{\alpha\beta}$ and $C_{\alpha\beta}$ must satisfy in order to define a surface is Gauss's *Theorema Egregium* [35]. It expresses the Gaussian curvature $K = \det C_{\alpha\beta}$ which is the determinant of the curvature tensor in terms of the Christoffel symbols. In the case of small and slowly varying strain (*i.e.* $\partial^2\gamma \gg (\partial\gamma)^2$) Gauss's theorem reads

$$\begin{aligned} K &= \partial_2\Gamma_{211} - \partial_2\Gamma_{212} + \Gamma_{11\rho}\Gamma_{\rho 22} - \Gamma_{12\rho}\Gamma_{\rho 21} \\ &= \partial_\alpha\partial_\beta\gamma_{\alpha\beta} - \nabla^2\gamma_{\rho\rho}, \end{aligned} \tag{2.5}$$

where $\nabla^2 = \partial_\mu\partial_\mu$. Summation over repeated indices is implied. Geometrically, the Gauss's equation captures the intuitive notion that non-zero Gaussian curvature (the sheet curves in both directions) must cause the sheet to strain. For historical reasons Eq. (2.5) in this context is usually referred to as the second von Kármán equation.

The other set of relations usually termed as Codazzi-Mainardi equations describes how the curvature tensor behaves when transported around a closed curve. Again, when the strains and consequently the Christoffel symbols are small these relations are simple. They say that if the curvature tensor is parallel transported around a closed curve, the change is of higher order in the strain [35]

$$\partial_\gamma C_{\alpha\beta} = \partial_\beta C_{\alpha\gamma}. \tag{2.6}$$

These equations are a tensor analogy of the condition satisfied by an irrotational vector field. And just as an irrotational vector field can be written as a gradient of a scalar, there exists a scalar function f such that

$$C_{\alpha\beta} = \partial_\alpha\partial_\beta f. \tag{2.7}$$

Equations Eq. (2.5) and (2.6) ensure that $C_{\alpha\beta}$ and $\gamma_{\alpha\beta}$ describe a physical surface. We now consider further conditions which assure that each element of the surface is in mechanical equilibrium. The forces and the torques acting on an infinitesimal element of the surface $\delta x\delta y$ from the rest of the plate can be found from the full three-dimensional stress tensor $\hat{\sigma}_{ij}$ where $i, j = 1, 2, 3$ (quantities without a hat will denote the moments of $\hat{\sigma}_{ij}$ with respect to the integration over the plate thickness.) This is where the expansion in the thickness as a small parameter takes place. If there

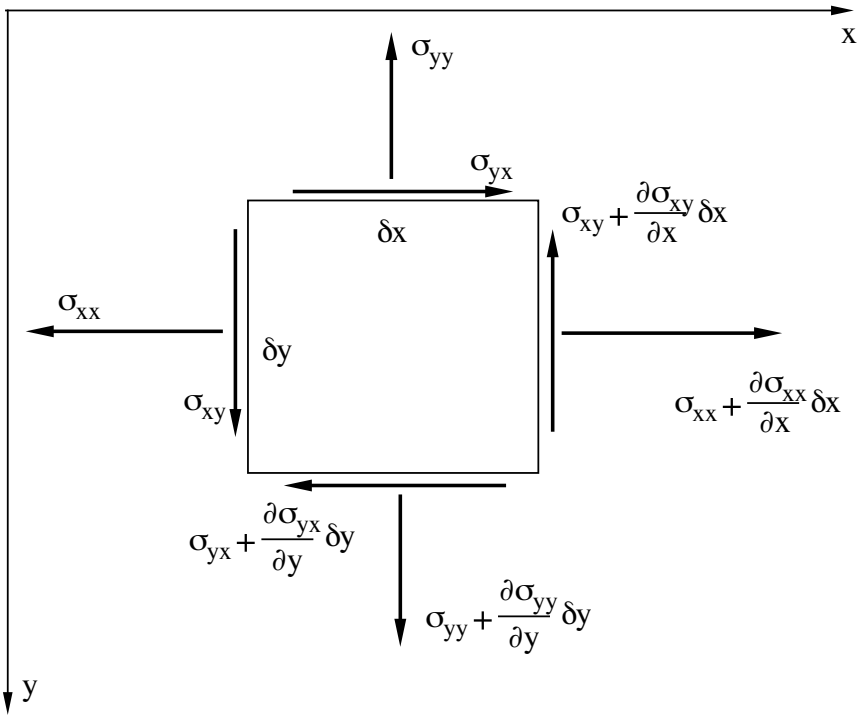

Figure 1. In-plane stresses (per unit length) acting on a small element of an elastic sheet obtained by integration of the three dimensional stress tensor over the thickness of the plate.

are no distributed external forces acting on the plate, the normal components of the stress tensor $\hat{\sigma}_{ij}(x, y, z)$ in the bent plate vanish on the top and bottom surfaces so that $\hat{\sigma}_{iz} = 0$ at $z = \pm h/2$. Here $z \in [-h/2, h/2]$ where h is the thickness of the plate is the coordinate perpendicular to the middle surface. Therefore, these components of the stress tensor are in some sense of higher order in the thickness as compared to the in-plane components $\hat{\sigma}_{\alpha\beta}$ $(\alpha, \beta = 1, 2)$. According to the rigorous derivations cited above, only the following moments of $\hat{\sigma}_{ij}$ are required to correctly capture the lowest order behavior of the bent plate. The in-plane stresses

$$\sigma_{\alpha\beta}(x, y) = \int_{-h/2}^{h/2} dz \ \hat{\sigma}_{\alpha\beta}(x, y, z), \tag{2.8}$$

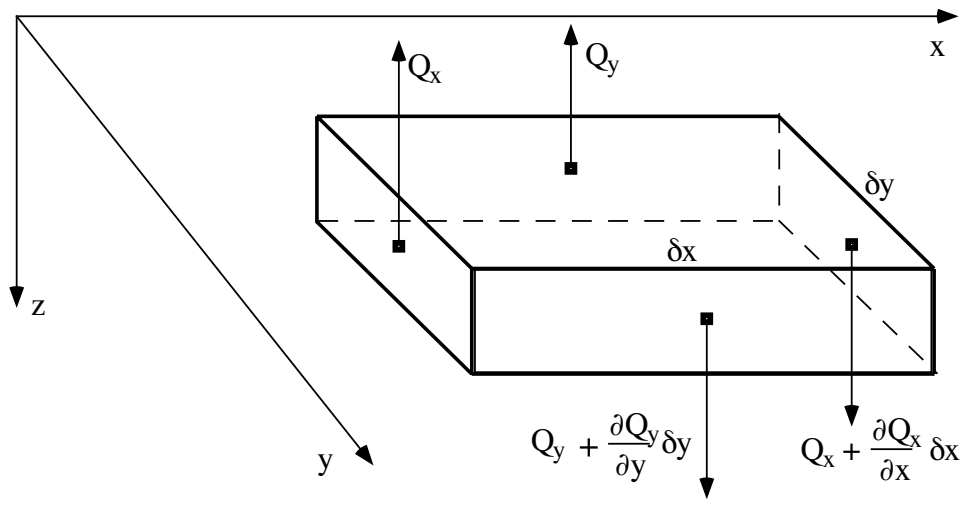

Figure 2. Normal shear stresses acting over the sides of the elementary area of the sheet.

are the forces on sides of the element $\delta x \delta y$ acting normal to the cross section of the plate as shown in Fig. 1. The normal shear stresses

$$Q_\alpha(x,y) = \int_{-h/2}^{h/2} dz\ \hat{\sigma}_{\alpha z}(x,y,z), \tag{2.9}$$

act over the sides of the element $\delta x \delta y$ in the direction normal to the plate as shown in Fig. 2. These forces are of higher order in the small expansion parameter since $\hat{\sigma}_{\alpha z}$ must vanish at $z = \pm h/2$. The first moments of the in-plane stresses

$$M_{\alpha\beta}(x,y) = \int_{-h/2}^{h/2} z dz\ \hat{\sigma}_{\alpha\beta}(x,y,z), \tag{2.10}$$

are of the same order in the strain as the normal shear stresses Q_α. They can be thought of as torques applied to the sides of the element $\delta x \delta y$ as shown in Fig. 3. Starting from a linear constitutive relation between the three dimensional stresses and three dimensional strains one can show [32] that the two dimensional in-plane stresses $\sigma_{\alpha\beta}$ and torques $M_{\alpha\beta}$ are also linearly related to the two dimensional strains $\gamma_{\alpha\beta}$ and curvatures $C_{\alpha\beta}$ respectively via

$$\sigma_{\alpha\beta} = \frac{Yh}{1-\nu^2}\left[\gamma_{\alpha\beta} + \nu \epsilon_{\alpha\rho}\epsilon_{\beta\tau}\gamma_{\rho\tau}\right] \tag{2.11}$$

$$M_{\alpha\beta} = \kappa\left[C_{\alpha\beta} + \nu \epsilon_{\alpha\rho}\epsilon_{\beta\tau}C_{\rho\tau}\right], \tag{2.12}$$

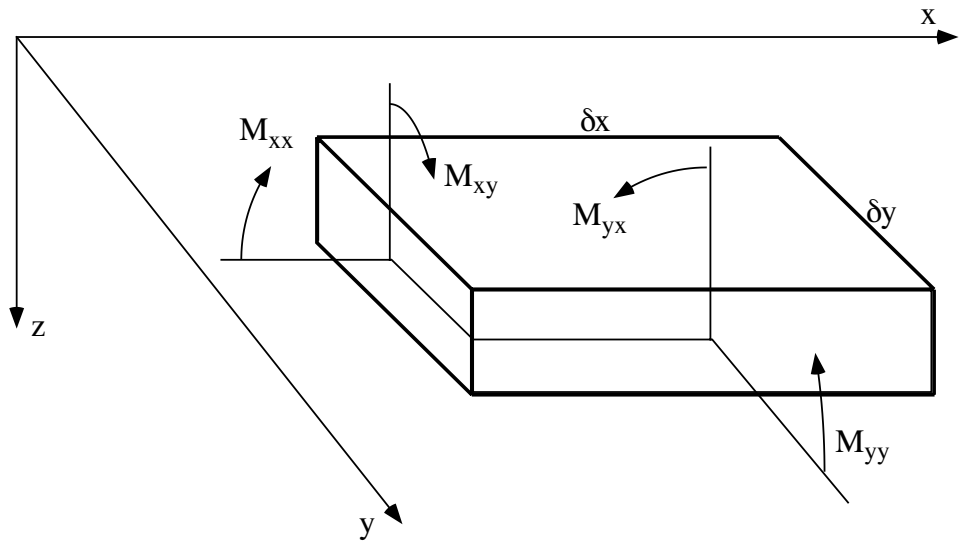

Figure 3. Bending and twisting torques per unit length acting on the element of the plate are first moments of the three dimensional stress tensor with respect to integration over the plate thickness.

where Y is the Young's modulus and ν is the Poisson ratio of the elastic material. $\kappa = Yh^3/(12(1-\nu^2))$ is called the bending rigidity of the plate [34]. Here $\epsilon_{\alpha\beta}$ is the two dimensional antisymmetric tensor.

The net force and torque on an element of the plate must vanish. The in-plane force balance gives to lowest nontrivial order in the strains

$$\partial_\alpha \sigma_{\alpha\beta} = 0. \tag{2.13}$$

We ignore higher order contributions, such as the in-plane components of the normal shear stresses Q_α which are non-zero due to the curvature of the element $\delta x \delta y$. Eq. (2.13) allows one to write the stresses in terms of a scalar potential $\chi(x,y)$ traditionally called the Airy force function,

$$\sigma_{\alpha\beta} = \epsilon_{\alpha\mu}\epsilon_{\beta\nu}\partial_\mu\partial_\nu\chi. \tag{2.14}$$

This relation is a tensor analog of the divergenceless vector field expressed as a curl of a vector potential.

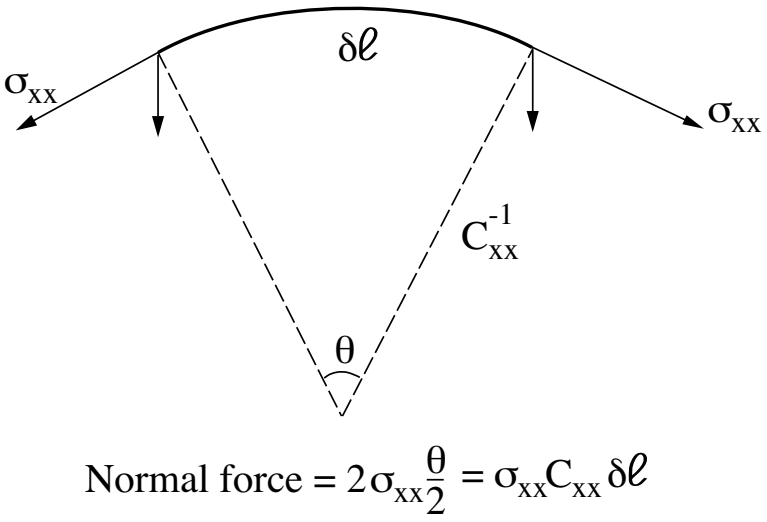

Figure 4. A one-dimensional derivation of the normal force on a curved element δl due to in-plane forces σ_{xx}

The balance of torques about the x- and y-axes relates the derivatives of the $M_{\alpha\beta}$ to the normal shear stresses Q_α via

$$Q_\alpha = \partial_\beta M_{\alpha\beta}. \tag{2.15}$$

Higher order contributions to the torques are again ignored.

In absence of distributed external loads, the resultant normal force on the element of the plate has two sources. First, the normal components of the in-plane tensions that act on the element are non-zero due to the curvature of the surface. It is easy to become convinced (see Fig. 4 for a one dimensional version of the derivation) that that normal force per unit area due to the in-plane tension is $\sigma_{\alpha\beta}C_{\alpha\beta}$ [32]. Second, a change in the normal shear stresses Q_α results in a net normal force per unit area of $\partial_\alpha Q_\alpha = \partial_\beta\partial_\gamma M_{\beta\gamma}$. A normal force balance is traditionally referred to as the first von Kármán equation

$$\partial_\alpha\partial_\beta M_{\alpha\beta} = \sigma_{\gamma\delta}C_{\gamma\delta}. \tag{2.16}$$

The more familiar form of the von Kármán equations emerges when one substitutes the potentials f and χ into Eqs. (2.5) and (2.16) using the constitutive relations Eq. (2.11) and the definition of the potentials. They read

$$\begin{aligned} \kappa\nabla^4 f &= [\chi, f] \\ \frac{1}{Yh}\nabla^4\chi &= -\frac{1}{2}[f, f], \end{aligned} \tag{2.17}$$

where we have defined

$$\begin{aligned} [a, b] &\equiv \epsilon_{\alpha\mu}\epsilon_{\beta\nu}(\partial_\alpha\partial_\beta a)(\partial_\mu\partial_\nu b) \\ &= \frac{\partial^2 a}{\partial x^2}\frac{\partial^2 b}{\partial y^2} + \frac{\partial^2 a}{\partial y^2}\frac{\partial^2 b}{\partial x^2} - 2\frac{\partial^2 a}{\partial x\partial y}\frac{\partial^2 b}{\partial x\partial y}. \end{aligned} \tag{2.18}$$

Notice that $[f, f]$ is twice the Gaussian curvature K.

In principle, the strains $\gamma_{\alpha\beta}$ and the curvatures $C_{\alpha\beta}$ obtained from the von Kármán equations as a function of the material coordinates define the surface uniquely (up to a rigid translation and rotation in $\mathbf{R}^3$). The problem of finding the shape of the surface from the strains and the curvatures is however highly nonlinear and intractable in general. One can make progress in a limited class of deformations in which the normal to the surface does not change much. In that case the so called Monge coordinates are appropriate. The undeformed plate is located in the $x - y$ plane so that upon deformation the point originally at $(x_1, x_2, 0)$ moves to $(x_1 + u_1, x_2 + u_2, w)$ in the 3-dimensional embedding space where u_α and w are functions of x_α. If the derivatives of u_α and w are small everywhere, only the lowest non-trivial order terms in those derivatives can be kept in the expressions for the strains and the curvatures. We obtain [34]

$$\gamma_{\alpha\beta} = \frac{1}{2}\left(\partial_\alpha u_\beta + \partial_\beta u_\alpha + \partial_\alpha w\partial_\beta w\right) \tag{2.19}$$

and

$$C_{\alpha\beta} = \partial_\alpha\partial_\beta w. \tag{2.20}$$

It is clear that the normal displacement w in this case is precisely the potential function f defined in Eq. (2.7).

To complete the description of the deformation of the thin elastic plate one needs to be able to calculate the elastic energy stored in the sheet and specify the boundary conditions on the functions f and χ. We begin by considering the work done on the small element of the surface $\delta x \delta y$ by the surrounding parts of the plate when the strain in the element changes by $\delta\gamma_{\alpha\beta}$. That work is $\sigma_{\alpha\beta}\delta\gamma_{\alpha\beta}\delta x\delta y$ [32]. The stretching energy $E_{\rm str}$ in the plate element is found by integrating the strain from 0 to its value $\gamma_{\alpha\beta}$ while keeping in mind that the stresses are proportional to the strains, which introduces a factor of 1/2. Thus the total stretching energy in the plate is given by

$$E_{\rm str} = \frac{1}{2}\int dxdy\ \sigma_{\alpha\beta}\gamma_{\alpha\beta}. \tag{2.21}$$

One can similarly show that the work done by the torques $M_{\alpha\beta}$ in bending a surface element is $\frac{1}{2}M_{\alpha\beta}C_{\alpha\beta}\delta x\delta y$ so that the total bending energy $E_{\rm bend}$ in the plate is [32]

$$E_{\rm bend} = \frac{1}{2}\int dxdy\ M_{\alpha\beta}C_{\alpha\beta}. \tag{2.22}$$

Expressing the strains, stresses, torques and curvatures in terms of the potentials χ and f we get after some algebra

$$E_{\rm str} = \frac{1}{2Yh}\int dxdy\ \left[{\rm tr}(\partial_\alpha\partial_\beta\chi)\right]^2 - 2(1+\nu){\rm det}(\partial_\alpha\partial_\beta\chi) \tag{2.23}$$

$$E_{\rm bend} = \frac{\kappa}{2}\int dxdy\ \left[{\rm tr}(\partial_\alpha\partial_\beta f)\right]^2 - 2(1-\nu){\rm det}(\partial_\alpha\partial_\beta f). \tag{2.24}$$

One can show that the conformation $\mathbf{r}(x,y)$ of the sheet which is a solution of the von Kármán equations minimizes the elastic energy while satisfying the boundary conditions [31]. We note in passing that many derivations of the von Kármán equations (see e. g. Ref. [11]) start with writing down these energies in an *add-hoc* way and then taking a variational derivative with respect to the sheet shape.

2.2. Boundary Layer Phenomena in Thin Plates and Shells

The von Kármán equations for thin shells are sometimes called the "interior" shell equations owing to the fact, pointed out by Green [36], that in general, not

all boundary conditions applied to the boundary edge surface S of the shell, when translated into the language of the two dimensional objects such as the stresses $\sigma_{\alpha\beta}$ and torques $M_{\alpha\beta}$, are compatible with the "interior" shell equations. Ref. [36] argues that in such cases one must solve the full three dimensional elasticity equation in a boundary layer whose size is of the order of the thickness of the shell in order to determine the correct boundary conditions for the "interior" shell problem. Boundary layers of this type with specific edge loading conditions were studied by several researchers. Kelvin and Tait [12] found that shear force, twisting moment, and bending moment combine to give effective Kirchhoff's boundary conditions for the "interior" shell problem.

A characteristic feature of all boundary layers of the type discussed above is that the solution to the interior shell equations with the effective boundary conditions exhibit strains of order unity in the boundary layer region thus invalidating the assumptions under which they were derived. We would like to focus our attention on a fundamentally different type of boundary layer phenomena in bending of thin plates and shells. There are situations in which the strains in the boundary layer remain small or vanish in the asymptotic limit of small shell thickness. This means that the von Kármán equations remain valid throughout the boundary layer region and thus correctly describe the asymptotic behavior of the stresses. Let us briefly discuss two such boundary layers.

Fung and Wittrick [37] discuss a boundary layer in bending and twisting of thin plates with free edges. They find that in the limit of small thickness, the shape of the bent plate is a piece of a cylinder (with Gaussian curvature identically zero) except in a narrow region of size $\delta \sim \sqrt{hX}$ near the edge. Here h is the thickness of the plate and X is its size. Outside the boundary layer region the shape of the plate can be determined by neglecting the bending rigidity altogether. This translates to omitting a term in the von Kármán equations. To see why that is true let us non-dimensionalize the von Kármán equations by defining

$$\bar{\chi} = \frac{\chi}{\kappa}, \quad \bar{f} = \frac{f}{X}, \quad \bar{x} = \frac{x}{X} \quad \text{and} \quad \bar{y} = \frac{y}{X} \tag{2.25}$$

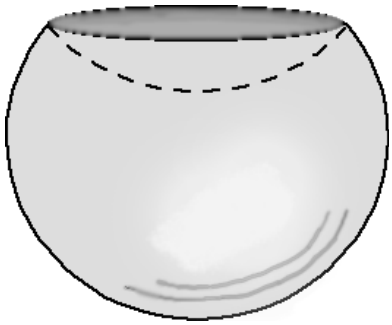

Figure 5. A ring ridge forms when a part of a spherical shell snaps through.

to obtain

$$\begin{aligned} \nabla^4 \bar{f} &= [\bar{\chi}, \bar{f}] \\ \lambda^2 \nabla^4 \bar{\chi} &= -\frac{1}{2}[\bar{f}, \bar{f}]. \end{aligned} \tag{2.26}$$

Here X is some characteristic length that describes the domain of the material coordinates or the geometry of the boundary conditions. The small parameter

$$\lambda \equiv \frac{\sqrt{\kappa/Yh}}{X} = \left(\frac{h}{X}\right) \frac{1}{\sqrt{12(1-\nu^2)}} \tag{2.27}$$

is proportional to the the dimensionless thickness of the plate. The membrane approximation, usually employed in the small thickness limit [32] starts with finding a solution of the *reduced* equations with $\lambda = 0$ that in general cannot satisfy the imposed boundary conditions. The boundary layer solution to the full von Kármán equations near the edge that matches onto the solution of the reduced equations is then sought to satisfy the boundary conditions.

Another boundary layer, that can be successfully described by the thin shell equations alone, occurs in axisymmetric buckling of a spherical shell [38]. When a large portion of the spherical shell snaps through, the solution to the reduced equations with bending rigidity set to zero is discontinuous along the ring edge as shown on Fig. 5. A boundary layer is therefore needed to correct the discontinuity at the sharp edge, *i.e.* to properly match the reduced solutions in the snap-through region and the rest of the sphere. The width of that boundary layer scales as $\sqrt{hR}$ where R is the radius of the sphere. The strains in the boundary layer again vanish

in the asymptotic limit of the small shell thickness thus allowing for a complete description with the thin shell equations.

2.3. Boundary Layers in a Crumpled Sheet

One of the approximate methods of dealing with the formidable complexity of the thin shell equations, that is applicable to very thin shells, is the membrane approximation. As noted above, in this method, the bending rigidity is set identically to zero, or equivalently, the 2D stretching modulus of the plate is considered infinite. Such a plate cannot stretch and must therefore be isometric to a plane. In other words, at each point of the surface, one the principle radii of curvature has to be infinite. Another way of seeing this is to go back to the reduced von Kármán equations (2.26) with $\lambda = 0$. It is clear that the second equation simply states that the Gaussian curvature $\frac{1}{2}[f, f]$ is identically zero. In differential geometry such surfaces are termed developable because there exists a set of the so-called generators–straight lines that lie in the surface.

It is possible to prove though, that a surface continuously embedded into a ball of a small enough radius cannot be developable [39]. Therefore, when a thin sheet is collapsed into a small ball, in the limit of the vanishing thickness, it assumes a piece-wise developable, or applicable shape. Therefore there are sharp creases where the developable pieces meet. These sharp creases converge at sharp points. Point singularities of this type were shown to arise in elastic plates in the limit of small thickness under quite general conditions [40]. A mechanism for the formation of these sharp point singularities has also been suggested in Ref. [41]. Just as in the case of a buckled sphere, discontinuities (sharp creases) in a reduced solution (with bending rigidity set to zero) are corrected by boundary layers. To determine the nature of these boundary layers, one must understand their geometry and effective boundary conditions that are responsible for their creation. Geometrically, there are few restrictions on the shape of the developable pieces and the creases at which they meet. The fact that the shape of a crumpled membrane is a minimizer of the elastic

energy functional, however, is likely to impose significant restrictions on the shape of the facets and creases in the limit of small plate thickness.

One of the asymptotic properties of these boundary layers is the amount of elastic energy in the region of the ridge. Presumably, the scaling of this energy with the dimensionless thickness λ differs for different types of ridges. Therefore, only the ridge type whose energy is lowest in the limit $\lambda \to 0$ will be found in a crumpled elastic sheet. This statement does not imply that a sheet finds the lowest energy configuration, quite the contrary, a crumpled membrane cannot explore all of its available configurations and is thus in a metastable state. However, if one fixes the degree of crushing (by say fixing the size of the ball into which the sheet has been confined) and then takes the limit $\lambda \to 0$, any ridge of a type that has a higher energy in that asymptotic limit will become unstable to breakup into ridges of the kind that have the lowest energy.

It is a conjecture that needs rigorous proof but is supported by numerical simulations [39], heuristic arguments, and everyday experience, that only *straight* ridges appear in crumpled sheets. It is plausible that the geometry of the crease determines the asymptotic scaling of its elastic energy. In particular, the limit of the Gaussian curvature on the crease is the deciding factor. For example, the Gaussian curvature on the the ring ridge of the buckled sphere described above tends to a derivative of a delta function. If the crease curve had non-zero torsion in addition to curvature (the ring ridge has zero torsion) the Gaussian curvature would approach a delta function. We will see later that in a straight ridge, Gaussian curvature approaches a finite constant on the ridge. We therefore hypothesize that in the limit of the vanishing thickness a crumpled sheet consists of flat facets that are bound by straight ridges that in turn meet at sharp vertices.

Regardless of whether the straight ridges correctly capture the structure of crumpled sheets, the scaling properties of the straight ridge singularity are of stand-alone scientific interest. The mechanism that controls ridges' behavior is similar to that of many singular phenomena some of which were mentioned above. Understand-

ing of the ridge singularities in thin elastic shells and plates therefore can provide a useful tool in studying other phenomena of this kind.

CHAPTER 3

BOUNDARY CONDITIONS INDEPENDENT PROPERTIES OF A STRAIGHT RIDGE

3.1. An Energy Scaling Argument

The essential ingredient for the formation of the straight ridge is the presence of the sharp vertices where the curvature is comparable to the inverse thickness of the plate. Ref. [41] argues that in the limit of small thickness when the surface is piecewise developable, a straight sharp crease connects these vertices. When the bending rigidity is taken into account, the crease relaxes to a characteristic radius of curvature C^{-1} governed by the competition of the bending and the stretching energies in the region of the ridge.

In order to reproduce the energy scaling argument, that determines the width of the ridge, let us rewrite the expressions for the elastic energies as

$$E_{\rm bend} = \frac{1}{2}\int dS\ (\kappa(C_1+C_2)^2 + \kappa_G C_1 C_2) \tag{3.1}$$

$$E_{\rm str} = \frac{1}{2}\int dS\ (G(\gamma_1+\gamma_2)^2 + G_s\gamma_1\gamma_2), \tag{3.2}$$

where, as above, C_β are the eigenvalues of the curvature tensor, and γ_β are the principal strains. κ_G is the Gaussian bending rigidity, $G = Yh$ is the 2D stretching modulus, and G_s is the shear modulus. For the purposes of an energy scaling argument we may ignore the second terms in the expressions for the energies.

The argument of Witten and Li of Ref. [42] assumes that the ridge can be described by a single parameter such as the characteristic curvature C. The bending $E_{\rm bend}$ and stretching $E_{\rm str}$ energies are then found with the following assumptions about the nature of the deformation in the $h \to 0$ limit as illustrated in Fig. 6. First, the bulk of the elastic energy is confined to a region of width C^{-1} around the ridge midline. Second, the midpoint of the ridge sags in the vertical direction by an

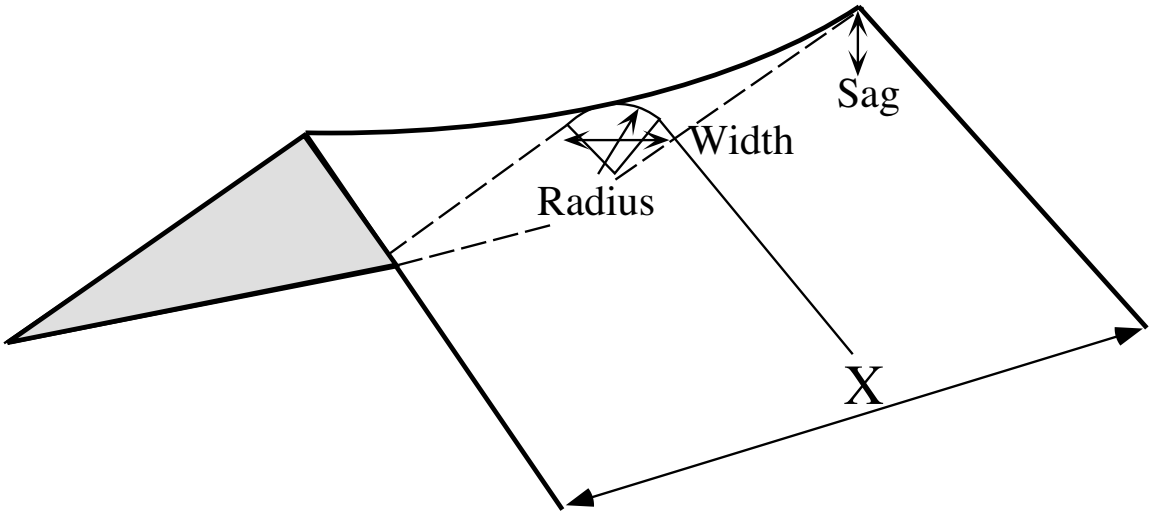

Figure 6. The energy scaling argument assumes that all of the energy is confined in a region of width C^{-1} around the ridge midline, that the ridge sags by an amount comparable to C^{-1}, and that the longitudinal strain in the ridge can be found by assuming that the vertices do not move closer to each other.

amount $d \sim C^{-1}$. Third, the vertices do not move closer together appreciably, so that if the length of the ridge, *i.e.* if the distance between the vertices is X, then the characteristic longitudinal strain $\gamma \sim (d/X)^2 \sim (CX)^{-2}$ exists in the ridge region. It turns out that the third assumption can be somewhat relaxed. Since, the crucial link in the scaling argument is the expression for the characteristic strain in terms of the ridge curvature, the vertices can not move a distance that is qualitatively greater than $X\gamma \sim C^{-2}X^{-1}$. Numerical simulations confirm that it is indeed the case. Ref. [41] gave further plausibility arguments to support the main assumption of energy confinement. We would like to stress that the only features of the ridge singularity utilized in this energy scaling argument are the existence of sharp vertices and the fact that the ridge is straight.

Thus, the total stretching energy in the ridge is approximately $E_{\rm str} \sim G\gamma^2(X/C) \sim GC^{-5}X^{-3}$. Similarly, the bending energy is given by the characteristic ridge curvature C, via $E_{\rm bend} \sim \kappa C^2(X/C) \sim \kappa CX$. Since both kinds of energy

vary as a power of C, they must be comparable when the total energy $E_{\rm bend} + E_{\rm str}$ is minimized. It immediately follows that

$$C \sim \left(\frac{G}{\kappa}\right)^{1/6} X^{-2/3} \sim h^{-1/3} X^{-2/3} \tag{3.3}$$

$$E_{\rm bend} \sim E_{\rm str} \sim \kappa \left(\frac{X}{h}\right)^{1/3}. \tag{3.4}$$

Another important conclusion of the energy scaling argument emerges when we consider the derivative of the energy with respect to the parameter C. It must vanish for the value of C at which the minimum total energy is achieved. Since the energies depend on powers of C we obtain the following statement

$$\frac{dE}{dC} = \frac{dE_{\rm str}}{dC} + \frac{dE_{\rm bend}}{dC} = \frac{-5E_{\rm str} + E_{\rm bend}}{C} = 0, \tag{3.5}$$

which leads to a "virial theorem" for ridges $E_{\rm bend} = 5E_{\rm str}$. The virial theorem is a direct consequence of the confinement of the elastic energy in the ridge assumed by the scaling argument. In other words, if one examines the bending and the stretching energy of a crumpled elastic sheet and finds that one is five times the other, the conclusion to be made is that ridges are well defined objects to which the scaling argument is applicable.

3.2. Dihedral Angle Scaling

To characterize the geometry of a ridge completely, its dihedral angle $\pi - 2\alpha$ in addition to its length X must be specified. From here on we will refer to α as the "dihedral angle" even though it is a half of the difference of the dihedral angle from π. Confusion is unlikely to result since this is the only way α is used in this work.

A scaling argument can be constructed to determine the dependence of the elastic energy, the ridge width, the ridge sag, and the mid-ridge strain on α when it is small $\alpha \ll 1$. The ridge curvature decays to zero at a finite distance from the ridge. We may, therefore, for the purposes of the scaling argument assume that the transverse profile of the ridge is and arc of a circle of radius C^{-1} that matches onto

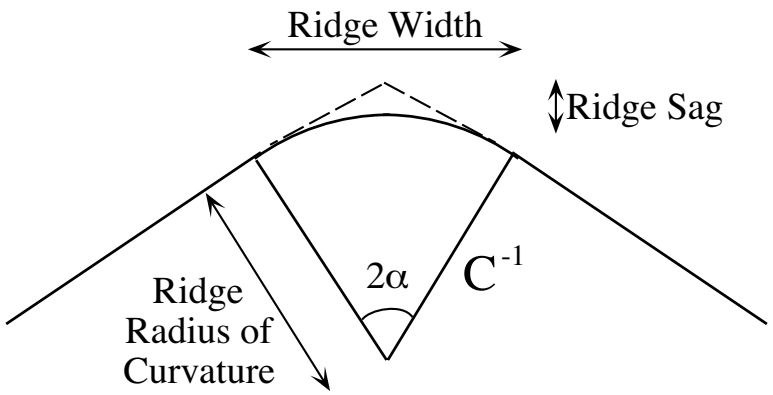

Figure 7. For the purposes of the dihedral angle scaling argument, the transverse ridge profile can be assumed to consist of an arc of a circle of radius C^{-1}. This allows one to determine the dependence of the ridge sag and the ridge width on the angle α.

straight flanks as illustrated in Fig. 7. Hence, the ridge width is $w \sim C^{-1}\alpha$. The ridge sag is then $d \simeq C^{-1}(1/\cos\alpha - 1) \sim C^{-1}\alpha^2$. The characteristic longitudinal ridge strain as before depends on the sag via $\gamma \sim (d/X)^2 \sim (CX)^{-2}\alpha^4$. Proceeding with the rest of the scaling argument as in the preceding section we obtain the dihedral angle scaling of the ridge energy E, the ridge curvature C, the ridge sag d, the ridge width w, and finally, the longitudinal strain γ

$$\begin{aligned} E &\sim \kappa\left(\frac{h}{X}\right)^{-1/3}\alpha^{7/3} \\ C &\sim X^{-1}\left(\frac{h}{X}\right)^{-1/3}\alpha^{4/3} \\ d &\sim X\left(\frac{h}{X}\right)^{1/3}\alpha^{2/3} \\ w &\sim X\left(\frac{h}{X}\right)^{1/3}\alpha^{-1/3} \\ \gamma &\sim \left(\frac{h}{X}\right)^{2/3}\alpha^{2/3}. \end{aligned} \tag{3.6}$$

These scaling predictions will be later put on a firmer ground by a boundary layer analysis of the von Kármán plate equations and confirmed numerically. Remarkably,

the scaling predictions Eqs. (3.6) are valid for all dihedral angles α despite the fact that the scaling derivation relied upon the angle α being small.

3.3. A Boundary Layer Solution of the von Kármán Equations

3.3.1. Definition of the Boundary Value Problem

The essential idea behind the scaling analysis of the ridge singularity is that in the asymptotic limit of the vanishing plate thickness, only a few geometric properties of the singularity, and not the detailed form of the boundary conditions, determine several quantitative properties such as the scaling exponents in Eq. (3.6). Therefore, any boundary value problem that exhibits the straight crease singularity in the small thickness limit must possess the above scaling behavior. In fact, the following boundary layer analysis does not make explicit use of the detailed form of the boundary conditions. Only the singularity of $\partial^2 f/\partial y^2$ at the boundary is used in Eq. (3.9).

We investigate the following boundary value problem that exhibits the ridge singularity. Consider a strip described in terms of material coordinates $(x, y) \in (-X/2, X/2) \times (-\infty, \infty)$ of uniform thickness $h \ll X$ made of isotropic homogeneous elastic material with Young's modulus Y and Poisson ratio ν. Normal forces are applied to the edge so as to bend the strip by an angle $\pi - 2\alpha$ as shown on Fig. 8. The membrane stresses $\sigma_{\alpha\beta}$ as well as the torques $M_{\alpha\beta}$ vanish at the boundary (except for the singular point $y = 0$). In terms of the potentials f and χ it means that

$$\partial_\alpha \partial_\beta f = \partial_\alpha \partial_\beta \chi = 0 \quad \text{at} \quad x = \pm \frac{X}{2}. \tag{3.7}$$

The condition that the strip is bent translates into specifying the curvature tensor at the boundary. We assume that the boundary is a geodesic of the surface which is reasonable in the small strain limit. In the direction along the boundary, the curvature is zero except for a sharp peak at the origin $y = 0$ where the strip is bent.

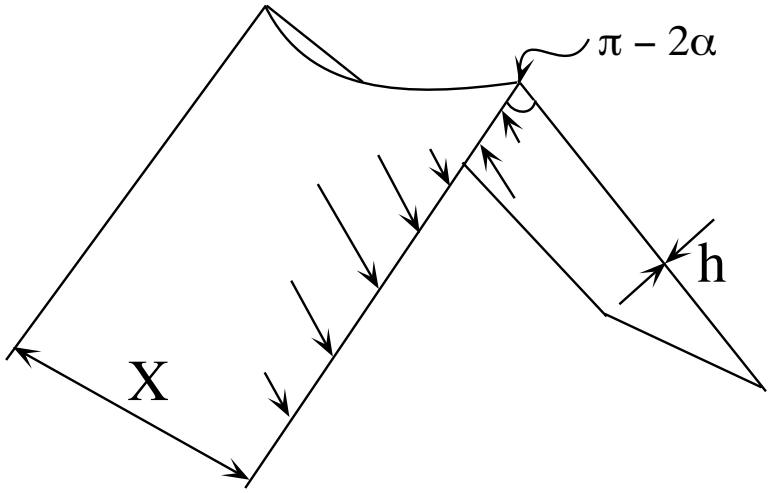

Figure 8. Normal boundary forces have been applied to an infinite strip of width X so as to bend it by an angle α.

The width of the bent region must be of the order of the thickness of the plate and the curvature is of the order of the inverse thickness. It is convenient then to set the curvature along the boundary to a δ-function since the all of the length scales in the problem are much larger than h. This leads to a particularly simple condition on f at the boundary

$$f(\pm X/2, y) = \alpha|y| \tag{3.8}$$

up to an arbitrary linear function of x_α.

To see that the coefficient α is identical to the bending angle introduced above consider the following integral along the boundary

$$\frac{\partial f}{\partial y}(\infty) - \frac{\partial f}{\partial y}(-\infty) = \int_{-\infty}^{\infty} dy\ \frac{\partial^2 f}{\partial y^2} = \int_{-\infty}^{\infty} dy \left|\frac{\partial \hat{\mathbf{n}}}{\partial y}\right| = 2\alpha, \tag{3.9}$$

where we have used the definition of the curvature tensor $C_{yy} = \partial_y \hat{\mathbf{n}} \cdot \hat{\mathbf{t}}_y$ and the fact that the integral is taken along a geodesic. Here $\hat{\mathbf{n}}$ is the unit normal and $\hat{\mathbf{t}}_y$ is tangent vector to the surface in the y-direction [35]. The geometric meaning of this integral is the length of the contour inscribed by the end of the normal vector $\hat{\mathbf{n}}$ on the unit sphere as $\hat{\mathbf{n}}$ is transported along the boundary. It is reasonable to believe

that the solution far away from the ridge approaches that of an unperturbed flat strip. Therefore, the derivative of the potential f along the transverse direction y does not depend on x far away from the ridge. Hence, the integral in Eq. (3.9) can be taken along any other geodesic which approaches $x = const$ far away from the ridge. This fact will later allow us to gain insight into the nature of dihedral angle dependence of the boundary layer solution.

3.3.2. Boundary Layer Scaling

The bent strip develops a sharp crease in the limit of the vanishing thickness. A boundary layer is thus needed to correct this singularity in the reduced solution. We use a standard treatment of boundary layers described in Ref. [43], for example. It involves a rescaling of all variables in Eqs. (2.26) by a power of the small parameter λ with the purpose of identifying the most important terms in the boundary layer region. Let us define

$$\bar{f} = \lambda^{-\beta}\tilde{f}, \quad \bar{\chi} = \lambda^{-\delta}\tilde{\chi}, \quad \bar{x} = \lambda^{0}\tilde{x}, \quad \bar{y} = \lambda^{-\beta}\tilde{y}. \tag{3.10}$$

Note that $\bar{x}$ remains unchanged by the rescaling transformation and $\bar{f}$ and $\bar{y}$ are rescaled by the same factor to satisfy the boundary condition Eq. (3.8). The rescaled equations read:

$$\begin{aligned} \lambda^{-\beta}\left[\frac{\partial^4\tilde{f}}{\partial\tilde{x}^4} + 2\lambda^{2\beta}\frac{\partial^4\tilde{f}}{\partial^2\tilde{x}\partial^2\tilde{y}} + \lambda^{4\beta}\frac{\partial^4\tilde{f}}{\partial^4\tilde{y}}\right] &= \lambda^{\beta-\delta}\,[\tilde{\chi},\tilde{f}] \\ \lambda^{2-\delta}\left[\frac{\partial^4\tilde{\chi}}{\partial\tilde{x}^4} + 2\lambda^{2\beta}\frac{\partial^4\tilde{\chi}}{\partial^2\tilde{x}\partial^2\tilde{y}} + \lambda^{4\beta}\frac{\partial^4\tilde{\chi}}{\partial^4\tilde{y}}\right] &= -\lambda^{0}\,\frac{1}{2}[\tilde{f},\tilde{f}]. \end{aligned} \tag{3.11}$$

The dominant terms in the $\lambda \to 0$ limit must be of the same order on either side of the equations. This leads unambiguously to $\beta < 0$ in agreement with the assumption that the width of the boundary layer must go to zero as the thickness of the sheet vanishes. Balance of the dominant terms gives

$$\beta = -\frac{1}{3} \quad \text{and} \quad \delta = \frac{2}{3}, \tag{3.12}$$

in agreement with the scaling argument of Witten and Li.

The rescaled equations are independent of λ in the $\lambda \to 0$ limit. Therefore, the rescaled quantities $\tilde{f}$ and $\tilde{\chi}$ and their derivatives with respect to $\tilde{x}$ and $\tilde{y}$ are finite in that limit. This fact allows one to obtain the small thickness behavior of such quantities as, for example, the transverse ridge curvature $C_{yy} = \partial^2 f/\partial y^2$ and the mid-ridge longitudinal strain $\gamma_{xx} = (1/Y)(\sigma_{xx} - \nu\sigma_{yy}) \simeq (1/Y)\partial^2\chi/\partial y^2$ where the expressions are evaluated at $x = 0$ and $y = 0$. The leading order behavior of the transverse stress $\sigma_{yy} = \partial^2\chi/\partial x^2$ is of higher order in λ and it thus can be ignored in the expression for γ_{xx}. Substituting the rescaled quantities we find that

$$C_{yy} = \frac{1}{X}\lambda^{-1/3}\frac{\partial^2\tilde{f}}{\partial\tilde{y}^2} \quad \text{and} \quad \gamma_{xx} = \lambda^{2/3}\frac{\partial^2\tilde{\chi}}{\partial\tilde{y}^2}. \tag{3.13}$$

These expressions give the asymptotic behavior of C_{yy} and γ_{xx} since the rescaled quantities do not depend on λ in the small λ limit. Since the longitudinal ridge curvature C_{xx} vanishes as $X\lambda^{1/3}$ in that limit, Gaussian curvature reaches a constant on the ridge midline. This result should be contrasted with the singular behavior of the Gaussian curvature for ridges with other geometries.

Note that the width of the boundary layer $w \sim y \sim X\lambda^{1/3}$ has the same leading order behavior as the radius of curvature of the plate at the center of the ridge and as the ridge sag which is the vertical deflection of the ridge middle from that of a perfectly sharp crease. This deflection is given by $f(0,0)$ in the small dihedral angle limit $\alpha \ll 1$. The sag can be found for a general dihedral angle α from the following argument. Due to the $x \to -x$ symmetry of the solution the ridge line $y = 0$ is a geodesic of the surface. Therefore we can relate the vertical deflection of the sheet $d(x)$ along the ridge to the curvature $C_{xx} = \partial^2 f/\partial x^2$. To lowest order in the strain we obtain

$$\frac{d''}{\sqrt{1-(d')^2}} = C_{xx} = \frac{\partial^2 f}{\partial x^2}. \tag{3.14}$$

Since C_{xx} vanishes in the limit of vanishing thickness, the leading term in the $\lambda^{2/3}$ expansion of $d''(x)$ scales with the same power of λ as $\partial^2 f/\partial x^2$. Thus the ridge sag

$d(0)$ is of the same order as the ridge width and as the mid-ridge transverse radius of curvature.

Let us now find the asymptotic behavior of the bending and stretching energies of the sheet. We first rewrite the expressions for the energies Eqs. (2.23) and (2.24) in terms of the non-dimensional variables

$$E_{\rm bend} = \kappa \int dxdy \ \left(\nabla^2 \bar{f}\right)^2 \tag{3.15}$$

$$E_{\rm str} = \kappa\lambda^2 \int dxdy \ \left(\nabla^2 \bar{\chi}\right)^2 . \tag{3.16}$$

The terms involving $\det(\partial_\alpha \partial_\beta f)$ and $\det(\partial_\alpha \partial_\beta \chi)$ can be expressed as an integral over the boundary [34]. These integrals vanish identically for the boundary conditions considered here. Substituting the rescaled quantities, which remain finite as $\lambda \to 0$, into Eqs. (3.15) and (3.16) we obtain

$$E_{\rm bend} = \kappa\lambda^{-1/3} \int d\tilde{x}d\tilde{y} \left(\frac{\partial^2 \tilde{f}}{\partial \tilde{y}^2}\right)^2 \tag{3.17}$$

$$E_{\rm str} = \kappa\lambda^{-1/3} \int d\tilde{x}d\tilde{y} \left(\frac{\partial^2 \tilde{\chi}}{\partial \tilde{y}^2}\right)^2 , \tag{3.18}$$

in agreement with the energy scaling argument of Witten and Li [42]. For a fixed thickness, these energies grow qualitatively slower (as $X^{1/3}$) than the energy of a sharp crease of size X that grows linearly with X.

3.3.3. Separation of Variables Ansatz

The solution to the rescaled equations (3.11) can be sought as an expansion in powers of $\lambda^{2/3}$,

$$\begin{aligned} \tilde{f} &= f_0 + \lambda^{2/3} f_1 + \lambda^{4/3} f_2 + \dots \\ \tilde{\chi} &= \chi_0 + \lambda^{2/3} \chi_1 + \lambda^{4/3} \chi_2 + \dots . \end{aligned} \tag{3.19}$$

Plugging the series into Eq. (3.11) and matching the coefficients of powers of $\lambda^{2/3}$ we can obtain equations for all orders in the $\lambda^{2/3}$ expansion. We get at zeroth order,

$$\begin{aligned} \frac{\partial^4 f_0}{\partial \tilde{y}^4} &= [\chi_0, f_0] \\ \frac{\partial^4 \chi_0}{\partial \tilde{y}^4} &= -\tfrac{1}{2}[f_0, f_0]. \end{aligned} \tag{3.20}$$

These equation differ from the full von Kármán equations by the absence of the dimensionless thickness λ. Also, the ∇^4 operator is replaced by $\partial^4/\partial\tilde{y}^4$ on the left hand side of the equations. We note in passing the equations for f_1 and χ_1. They read

$$\begin{aligned} \frac{\partial^4 f_1}{\partial \tilde{y}^4} + 2\frac{\partial^4 f_0}{\partial \tilde{x}^2 \partial \tilde{y}^2} &= [\chi_0, f_1] + [\chi_1, f_0] \\ \frac{\partial^4 \chi_1}{\partial \tilde{y}^4} + 2\frac{\partial^4 \chi_0}{\partial \tilde{x}^2 \partial \tilde{y}^2} &= -[f_0, f_1]. \end{aligned} \tag{3.21}$$

At this point we must draw the readers' attention to the fact that while $\tilde{f}$ and $\tilde{\chi}$ satisfy the boundary conditions Eq. (3.7) and Eq. (3.8) there is no reason to expect that f_0 and χ_0 do. In fact, numerical evidence hints that f_0 and χ_0 have little direct connection with the boundary conditions for f and χ except in the case of $y \to \infty$. In other words, it is likely that the expansion in powers of $\lambda^{2/3}$ does not converge uniformly, so that for a fixed λ higher orders in the expansion Eq. (3.19) become increasingly important as the boundary is approached. As a result, the solution of the zeroth order equations (3.20) might therefore be a good approximation to $\tilde{f}$ and $\tilde{\chi}$ only in a restricted area around the ridge away from the boundaries. In addition, a substitution of the series into the expression for the elastic energy must be done with caution. One cannot, in general, interchange the order of summation and integration when integrating non-uniformly converging series. Thus, individual terms in the series Eq. (3.19) when substituted into Eqs. (3.15) and (3.16) may yield diverging integrals. The leading order behavior of the elastic energy is found correctly, however, since that claim did not depend on the series expansions of f and χ.

To help solve equations (3.20) we observe that the boundary conditions do not introduce another length scale to the problem. Therefore, the transverse profile

of the ridge ought to *scale* with the distance from its midpoint $\tilde{x} = 0$. In other words, different $\tilde{x} = const$ slices of the strip are similar and can be made to coincide by an appropriate rescaling of the axes. In a mathematical language, one must find a functional form of f_0 and χ_0 such that the different $\tilde{x} = const$ slices are related to each other by a scale factor $q(\tilde{x})$ that depends on $\tilde{x}$ only. By assuming scaling in $\tilde{x}$ we hope to decouple it from the new transverse variable $\xi = \tilde{y}/q(\tilde{x})$. We assume that

$$f_0(\tilde{x}, \xi) = q^{\mu}(\tilde{x}) p_1(\xi), \qquad \chi_0(\tilde{x}, \xi) = q^{\eta}(\tilde{x}) p_2(\xi). \tag{3.22}$$

To show that Eqs. (3.20) separate only when $\mu = \eta = 1$ we carry out the substitution for general exponents. We obtain

$$\begin{aligned} p_1'''' &= q'' q^{\eta+1} \left[\eta p_1'' p_2 + \mu p_2'' p_1 - \xi (p_1'' p_2' + p_2'' p_1')\right] + \\ &\quad + (q')^2 q^{\eta} \left\{(\eta - 1)\eta p_1'' p_2 + \mu(\mu - 1) p_2'' p_1 - 2(\mu - 1)(\eta - 1) p_1' p_2'\right\} \qquad (3.23) \\ p_2'''' &= -q'' q^{2\mu - \eta + 1} \left[\mu p_1'' p_1 - \xi p_1'' p_1'\right] + \\ &\quad + (q')^2 q^{2\mu - \eta} \left\{(\mu - 1)^2 (p_1')^2 - \mu(\mu - 1) p_1'' p_1\right\} \qquad (3.24) \end{aligned}$$

The separation of variables conditions on the scale function $q(\tilde{x})$ demand that $q'' q^{\eta+1} = A_1$ and $q'' q^{2\mu-\eta+1} = A_2$ which requires that $\mu = \eta$. Unless the factors in curly braces vanish, separability also demands that $(q')^2 q^{\eta} = A_3$ and $(q')^2 q^{2\mu-\eta} = A_4$. From the A_1 and A_3 conditions it follows that $q'' q = (A_1/A_3)(q')^2$ which implies that $q' \propto q^{A_1/A_3}$. Since we require that $q'(0) = 0$ and $q(0) \neq 0$, one of the following two conditions must be true. First A_1 may vanish which leads to an unphysical choice $q'' \equiv 0$. Second, the factors in curly braces may vanish which happens only if $\mu = \eta = 1$. We conclude that indeed $\mu = \eta = 1$ is the only choice for which variables separate. This choice of the scaling exponents in the $q(\tilde{x})$-scaling of the solution to the rescaled equations implies that width of the ridge solution scales with the distance from the vertex in the same way as the ridge sag. As mentioned above, the boundary conditions on f require that its transverse derivative $\partial f/\partial y$ approach a constant independent of x. If a similar condition is to hold for f_0 then inescapably $\mu = 1$. The validity of the $q(\tilde{x})$-scaling hypothesis needs to be corroborated by some other means. In section 3.4

we present numerical evidence supporting the $q(\tilde{x})$-scaling ansatz, here we only note that this evidence is convincing.

Substitution of the ansatz Eq. (3.22) with $\mu = \eta = 1$ into the zeroth order equations (3.20) gives

$$p_1'''' = q''q^2\left[p_1''p_2 + p_2''p_1 - \xi(p_1''p_2' + p_2''p_1')\right] \tag{3.25}$$

$$p_2'''' = -q''q^2\left[p_1''p_1 - \xi p_1''p_1'\right]. \tag{3.26}$$

Separation of variables provides the equation for the scale factor $q''q^2 = A$, where A is some constant. This equation, together with the condition that $q(\tilde{x})$ be even can be solved by a substitution $g(q) = q'(\tilde{x})$ to yield,

$$\tilde{x} = \frac{1}{\pi}\left[\frac{\pi}{2} - \arcsin\sqrt{\frac{q(\tilde{x})}{q(0)}} + \sqrt{\frac{q(\tilde{x})}{q(0)}\left(1 - \frac{q(\tilde{x})}{q(0)}\right)}\right], \tag{3.27}$$

where the separation of variable constant is related to $q(0)$ via $A = -\pi^2 q^3(0)/2$. The scale factor $q(\tilde{x})$ has a singular derivative near the vertices, since for $\tilde{x} = 1/2 - \epsilon$

$$q(\epsilon) \simeq \left(\frac{3\pi}{2}\right)^{2/3}\epsilon^{2/3}, \tag{3.28}$$

which is consistent with the suspicion that the series expansion (3.19) does not converge uniformly. Numerical simulations of the ridge show, however, that the scale factor $q(\tilde{x})$ correctly captures the shape of the ridge midline away from the vertices.

3.3.4. Transverse Ridge Shape

The separation of variables ansatz implies that once $q(0)$ (related to the ridge sag) has been specified, the shape of the ridge midline is asymptotically independent of the details of the boundary conditions, since nowhere in the derivation were these details utilized. The transverse ridge profile p_1 and p_2, however, does depend on the detailed form of the boundary conditions. To see that we make the following transformation to the new functions $\phi_\beta(\xi)$ for $\beta = 1, 2$ via

$$\phi_\beta(\xi) = p_\beta(\xi) - \xi p_\beta'(\xi). \tag{3.29}$$

The functions p_α can then be readily found from

$$p_\beta(\xi) = G_\beta \xi + \xi \int_\xi^\infty d\zeta \frac{\phi_\beta(\zeta)}{\zeta^2}, \tag{3.30}$$

where where G_β are integration constants. This transformation allows one to integrate the transverse equations (3.26) once. We obtain

$$\begin{aligned} \phi_1'' - \frac{2}{\xi}\phi_1' &= A\phi_1\phi_2 + D_1 \\ \phi_2'' - \frac{2}{\xi}\phi_2' &= -\frac{1}{2}A\phi_1^2 + D_2. \end{aligned} \tag{3.31}$$

Here D_β are the integration constants (different from G_β) allowing for a non zero asymptote of the functions ϕ_β. The large ξ behavior of ϕ_β depends on whether the integrals of the right hand sides of Eqs. (3.31) are finite. If they diverge, ϕ_β also diverge in the $\xi \to \infty$ limit as some powers of ξ. This behavior is clearly unphysical. If, on the other hand, these integrals are finite, ϕ_β have well defined averages determined by D_β in the $\xi \to \infty$ limit. The deviations of ϕ_β from these average values must remain finite for large ξ. Suppose that these deviations vanish asymptotically. Then, an expansion around the average values of ϕ_β for large ξ yields a system of linear ordinary differential equations. This implies that ϕ_β approach their asymptotic constant values exponentially fast. The finite limit of ϕ_β as $\xi \to \pm\infty$ would imply a finite stress and curvature far away from the ridge. However, since we expect the series Eq. (3.19) to converge non-uniformly, the large ξ behavior of ϕ_β is likely to be unphysical.

What makes solving the transverse zeroth order equations (3.31) difficult if not impossible is the fact that they contain non-universal constants D_1 and D_2 that carry information about the large ξ behavior of ϕ_1 and ϕ_2 that depends not only on the boundary conditions for f and χ, but also on the behavior of the higher order terms in the $\lambda^{2/3}$ expansion Eq. (3.19). Let us, nevertheless, discuss the behavior of the functions ϕ_β near the boundaries and ways in which it may be connected with the boundary conditions for the ridge. The second derivatives of f_0 (and χ_0),in terms of which the boundary conditions may be given, read

$$\frac{\partial^2 f_0}{\partial \tilde{y}^2} = -\frac{1}{\xi q}\phi_1', \qquad \frac{\partial^2 f_0}{\partial \tilde{x}\partial \tilde{y}} = \frac{q'}{q}\phi_1', \qquad \frac{\partial^2 f_0}{\partial \tilde{x}^2} = q''\phi_1 - \frac{q'^2\xi}{q}\phi_1'. \tag{3.32}$$

The boundary of the strip $x = \pm X/2$ is mapped onto the $\xi \to \pm\infty$ segments plus the "special" points $\xi = 0$. Note that since ϕ'_α decays exponentially for large ξ the only concern in satisfying boundary conditions is the behavior of the $q''\phi$ term in $\partial^2 f_0/\partial x^2$. For $x \neq \pm X/2$ and $y \to 0$ that term reaches a constant. It diverges when x approaches the boundary $x = \pm X/2$ for a finite y. Problems could also arise at the "special" points $\xi = 0$, $x = \pm X/2$ since q goes to zero there, and q' and q'' diverge. It is evident that near these "special" points knowledge of higher order terms in the $\lambda^{2/3}$ expansion is needed to determine boundary condition dependence of the zeroth order term in the expansion.

Let us for the moment consider only the $\xi \to \infty$ boundary conditions. We might at first assume that all of the higher order functions in the $\lambda^{2/3}$ expansion obey $q(\tilde{x})$-scaling with the same $q(\tilde{x})$. Then, from Eq. (3.32) we deduce that all of the second derivatives of f_0 (and χ_0) will vanish in that limit if

$$0 = lim_{\xi\to\infty} \sum_j \phi_\alpha^{(j)}(\xi)\lambda^{2j/3}. \tag{3.33}$$

This is possible despite the fact that the individual terms in the series may diverge in that limit. The sum must vanish for large ξ fast enough to overcome the divergence of the q'' term as the boundary is approached.

As far as the "special" vertex points $\xi = 0$ are concerned, it seems that the situation is much worse. All three second derivatives in Eq. (3.32) diverge. The remedy might lie in considering the full expansion as above and also in remembering that some of the second derivatives must diverge at the vertex because the boundary condition for f itself is singular there. The real reason for these difficulties is that the conditions of validity of the thin plate equations are violated near the vertices so that the full three dimensional elasticity must be invoked there.

The simplicity and the apparent symmetry of the Eqs. (3.31) must point to some physical symmetry in the problem that forces this behavior to occur. Perhaps further light can be shed onto the physical meaning of the functions ϕ_β by writing

down the expression for the elastic energy of the sheet in terms of the separable solution. The leading term in the $\lambda^{2/3}$-expansion of the total elastic energy reads

$$\begin{aligned} E &= \int d\tilde{x}d\tilde{y}\frac{1}{q^2}\left((p_1'')^2+(p_2'')^2\right) \\ &= \int \frac{d\tilde{x}}{q(\tilde{x})}\int \frac{d\xi}{\xi^2}\left[\left(\frac{d\phi_1}{d\xi}\right)^2+\left(\frac{d\phi_2}{d\xi}\right)^2\right]. \end{aligned} \tag{3.34}$$

One can make contact with the boundary condition $\tilde{f}\to\alpha|\tilde{y}|$ as $\tilde{y}\to\infty$. The coefficient of the linear growth of f_0 must be the same as that of f far away from the ridge. Therefore, if the integral in Eq. (3.30) converges, this boundary condition gives $G_1=\alpha$. Now one can use the $y\to -y$ symmetry of the problem and sufficient smoothness of functions involved to conclude that $p_1'(0)=0$ which leads to

$$\int_0^\infty \frac{d\zeta}{\zeta}\frac{d\phi_1(\zeta)}{d\zeta}=-\alpha. \tag{3.35}$$

3.3.5. Dihedral Angle Scaling of the Separable Solution

Even without having solved the transverse equations one can deduce the behavior of the solution for different dihedral angles α just from the form of the Eqs. (3.31). We begin by noting that there exists a two-parameter family of transformations that produce new solutions. For example if $\vec{\phi}(\xi)$ is a two-component solution, then $\vec{\psi}(\xi)=S_1\vec{\phi}(S_2\xi)$ is also a solution of the equations (3.31) but with a different separation of variable constant $A'=S_2^2/S_1A$. We must allow for variation of A since it will undoubtedly depend on the dihedral angle. Using the boundary condition on ϕ_1 Eq. (3.35) we can find the corresponding dihedral angle $\alpha'=S_1S_2\alpha$. With this condition, there is a one-parameter family of scale transformations which produce a solution for the dihedral angle α' given that for the dihedral angle α. Let us fix a reference solution $\vec{\phi}_0$ with $\alpha=1$ so that all other solutions are labeled by the scale

factors S_1 and S_2. We can now find how various quantities of interest are affected by the scale transformation. We start with the simplest cases

$$\begin{aligned} \alpha &\sim S_1 S_2 \\ p_1 \sim p_2 &\sim S_1 \\ q \sim A^{1/3} &\sim S_1^{-1/3} S_2^{2/3}. \end{aligned} \tag{3.36}$$

The relevant quantities such as the ridge sag $d \sim q p_1$, the transverse curvature in the middle of the ridge $C \sim (1/q) p_1''$, both evaluated at $\tilde{x} = \xi = 0$, and the elastic energy E from Eq. (3.34) all turn out to depend only on the product of the scaling factors $S_1 S_2$ which unambiguously determines their scaling with the dihedral angle α. Using Eqs. (3.36) we get

$$\begin{aligned} d \sim q p_1 &\sim S_1^{-1/3} S_2^{2/3} S_1 &&\sim \alpha^{2/3} \\ C \sim (1/q) p_1'' &\sim S_1^{1/3} S_2^{-2/3} S_1 S_2^2 &&\sim \alpha^{4/3} \\ E \sim \int \frac{d\tilde{x}}{q(\tilde{x})} \int \frac{d\xi}{\xi^2} \left(\frac{d\phi}{d\xi} \right)^2 &\sim S_1^{1/3} S_2^{-2/3} S_1^2 S_2^3 &&\sim \alpha^{7/3}, \end{aligned} \tag{3.37}$$

in agreement with the dihedral angle scaling argument of Sec. 3.2.

One can also predict how the width of the ridge w which scales as S_2^{-1} depends on the dihedral angle α. Since the transverse curvature decays exponentially away from the ridge, the width of the ridge scales as the radius of curvature times the bend angle α. Therefore

$$w \sim S_2^{-1} \sim \alpha C^{-1} \sim \alpha^{-1/3}. \tag{3.38}$$

This equation fixes the dependence of the scale factors S_1 and S_2 on α so that solutions for all dihedral angles can be generated from a single solution for some α. All of the α-scaling predictions have been convincingly verified by the numerics.

3.4. Numerical Simulation of the Stretching Ridge

3.4.1. The Lattice Model

We have used a lattice model of an elastic sheet introduced by Seung and Nelson [11]. An elastic sheet is modeled as a triangular lattice of springs of unstretched

length a and spring constant K after Ref. [11]. Bending rigidity is introduced by assigning an energy $J(1-\hat{\mathbf{n}}_1\cdot\hat{\mathbf{n}}_2)$ to every pair of adjacent lattice triangles with normals $\hat{\mathbf{n}}_1$ and $\hat{\mathbf{n}}_2$. Seung and Nelson showed that when strains are small and the radii of curvature are large compared to the lattice constant, this model membrane bends and stretches as a sheet of thickness $h = a\sqrt{8J/K}$ made of isotropic homogeneous elastic material with Young's modulus $Y = 2Ka/(h\sqrt{3})$ and Poisson ratio $\nu = 1/3$. The bending modulus is $\kappa = J\sqrt{3}/2$. It turns out that the Gaussian bending rigidity κ_G introduced earlier is not correctly captured by this lattice model. Gaussian bending energy, however, is not relevant for closed shapes without edges, for which it is a topological invariant [35]. In addition, this energy can be expressed as an integral over the strip's boundary. For the boundary conditions that were implemented in this work, the boundary integral vanishes.

The lattice model mimics the energy functionals Eqs. (2.23) and (2.24). Equilibrium shapes of this model, therefore, are solutions of the von Kármán equations since the energies were a direct consequence of these equations. A numerical test of the asymptotic scaling predictions with the lattice model can only test the correctness of the scaling analysis and not the validity of the von Kármán equations themselves. To administer such a test one would have to introduce a lattice model for a three dimensional elastic solid and then make it into a thin sheet.

A variety of shapes that exhibit a sharp vertices connected by ridges in the limit of small thickness were made by either introducing disclinations or applying appropriate boundary conditions. We studied a regular tetrahedron shape shown in Fig. 9 that includes four disclinations of charge π (defined as the integrated Gaussian curvature), a "boat" shape shown in Fig. 10 that is a sheet with two disclinations of charge $\pi/3$, and a "bag" shape shown in Fig. 11 that is a cylinder with one end sewn shut. The bag shape contains two disclinations of charge π. We also applied forces to the boundary particles of a rhombus shaped piece (see Fig. 12 of the simulated material and a rectangular piece so as to bend them by an angle $\pi - 2\alpha$.

Shading in the pictures is proportional to the stretching energy density. The stretching energy oscillates as one moves away from the ridge line rather than going

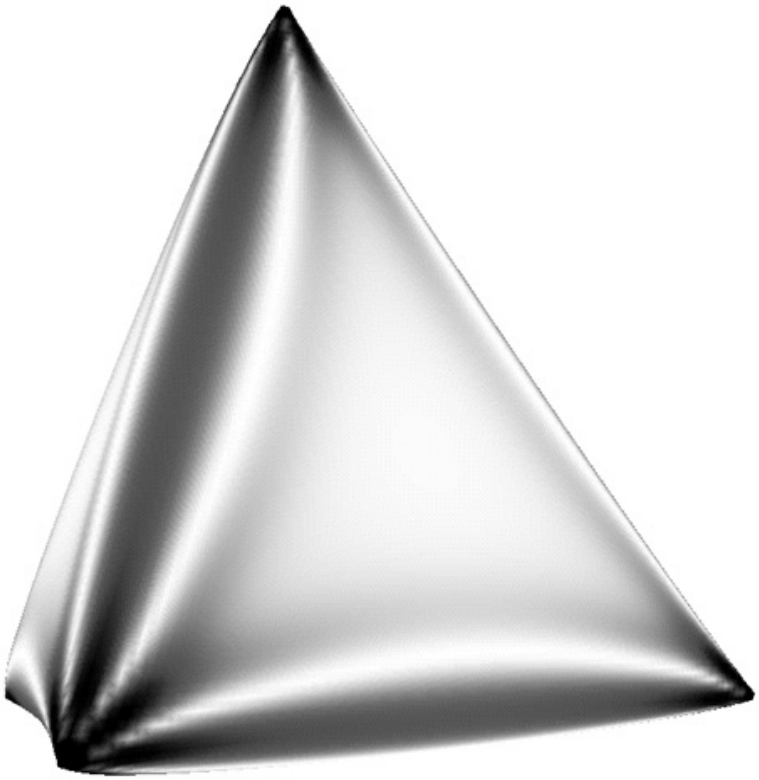

Figure 9. A regular lattice tetrahedron of size $X = 100a$ and elastic thickness $h = a/27.4$; shading is proportional to the stretching energy density.

Figure 10. A two-vertex boat shape with $X = 67.48a$ and $h = a/20.4$ The two vertices are of "sharpness" (disclination charge or integrated Gaussian curvature) $\pi/3$.

monotonically to zero. This is not surprising since the transverse behavior of the ridge shape and stresses is a solution of the second order ordinary differential equations of the "oscillatory kind," *i.e.* the sign of the second derivatives of ϕ_β in Eqs. (3.31) are such as to curve ϕ_β toward the ξ axis. For the shapes with a free edge (Figs. 10 and 11), there are regions of large curvature at the free edge opposite to the vertices. Faint induced ridges appear between the vertices and the induced "vertices" at the edges. These induced features become stronger as the dimensionless thickness λ decreases.

We used a conjugate gradient routine to find a number of minimum energy shapes with a range of geometric parameters such as the length of the bag, the dihedral angle of the bent strip, and the dimensionless thickness λ. We measured the ridge curvature, the longitudinal strain, the elastic energy, the sag, the vertex-to-vertex distance, and the longitudinal and the transverse curvature profiles to be compared with the predictions of the preceeding sections.

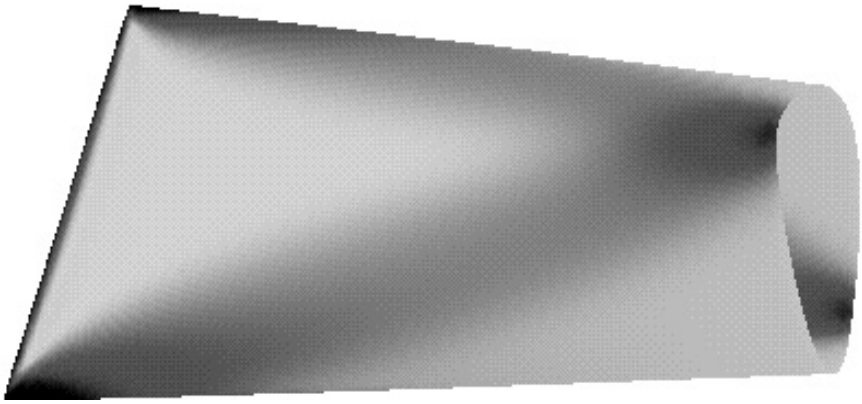

Figure 11. A two-vertex bag shape with the ridge of length $X = 50a$, thickness $h = a/27.4$, and the length of $2X$. The sharpness of the vertices is π as in a regular tetrahedron.

Figure 12. A kite shape made from a flat, rhombus-shaped surface by exerting normal forces on the perimeter sites. The forces constrain the perimeter to follow a rectilinear frame with dihedral angle α equal to that of the tetrahedron, namely $\cos^{-1}(1/3)$. Ridge length is $X = 100a$ and thickness is $h = a/13.7$.

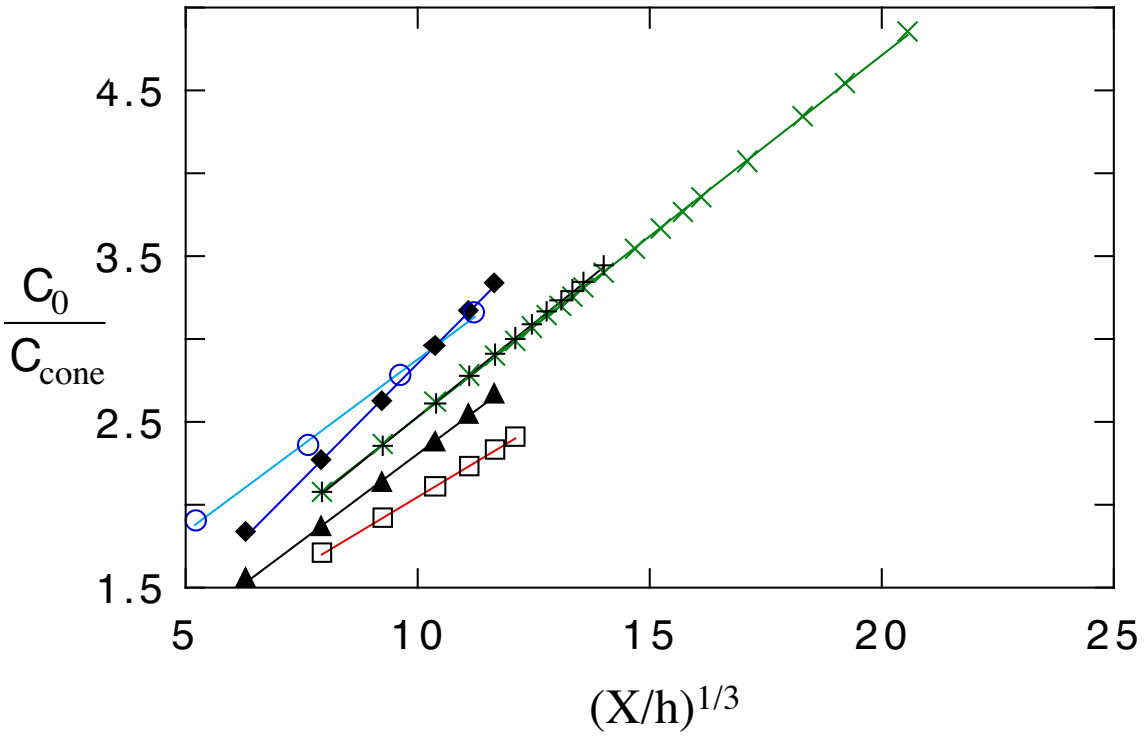

Figure 13. Mid-ridge curvatures for simulated surfaces, relative to the curvature of a single cone at the same distance from its vertex. Horizontal axis is the anticipated scaling variable $(X/h)^{1/3}$. Open squares, kite shapes; open circles, boat shapes; closed triangles, bags with ridge of length $X = 50a$ and skirt length of X; closed diamonds, bags of twice as long a skirt $2X$; plusses, tetrahedra with ridge length $X = 50a$; x's, tetrahedra with ridge length $X = 100a$. Straight lines indicate the anticipated scaling behavior.

3.4.2. A Test of the Scaling Predictions

We first tested the dependence of the mid-ridge curvature on the dimensionless thickness $\lambda \sim h/X$. In Fig. 13 we plot the transverse curvature $C_{yy}(0,0) = C_0$ *vs.* the predicted scaling variable $(X/h)^{1/3}$ for different shapes. The curvature is expressed relative to the curvature at the same point if only one vertex were present (which is proportional to X^{-1}). We note first that the curvatures follow the anticipated $(X/h)^{1/3}$ scaling. The tetrahedron has a reduced curvature of $0.22(X/h)^{1/3}$, as determined from fitting all the data. The uncertainty in this coefficient derived from the scatter of the data is less than 0.001. Second, the slopes and the intercepts of the straight lines on the graph depend on the dihedral angle α of the ridge as well as the details of the boundary conditions. For example, the ridges in the bag shapes of different length have effectively different dihedral angles and thus show a different slope in the ridge curvature scaling. Third, in all cases, the ridge begins to dominate the curvature (doubling the curvature as compared to that of a single cone) for X/h in the range of 350 to 1000.

We analyzed the tetrahedral shape in greater detail. We first verified that the shapes were independent of lattice size for a fixed λ. The curvature at mid-ridge differs from the extrapolation to an infinitely fine lattice by no more than two percent. Since our results are insensitive to the lattice spacing for a given thickness, they are not sensitive to the details of the lattice model used, but would hold quantitatively for any elastic material. The transverse curvature profile shrinks inward with decreasing λ which is consistent with the assumption of elastic energy confinement. The shrinkage is consistent with the anticipated $(h/X)^{1/3}$ scaling. This can be seen by plotting the mean-squared curvature across the ridge as shown in Fig. 14 for four different thicknesses. The ridge profiles collapse onto a single scaling curve.

We also tested the assumption, made in the energy scaling argument, about the movement of the vertices and the implication of that negligible vertex movement for the scaling of the mid-ridge strain. In Fig. 15 we plot the fractional vertex-to-vertex movement and the longitudinal ridge strain for a tetrahedral shape with the

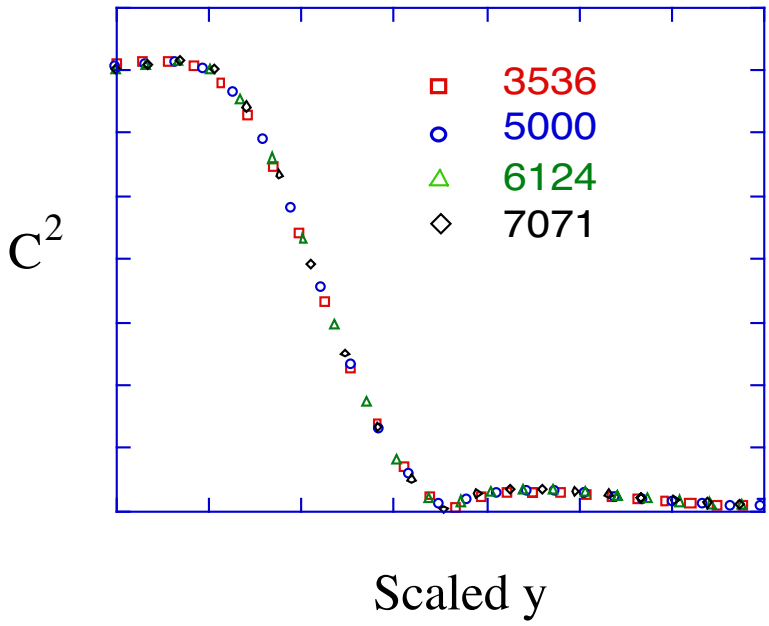

Figure 14. Squared transverse ridge curvature C_{yy}^2 of the lattice tetrahedra scaled by $X^{-2}(X/h)^{2/3}$ along the perpendicular bisector of the ridge. The distance y from the ridge is scaled by $X(X/h)^{-1/3}$. The legend indicates the size to thickness ratios X/h used. Longitudinal strain profile $\gamma_{xx}(y)$ is similar.

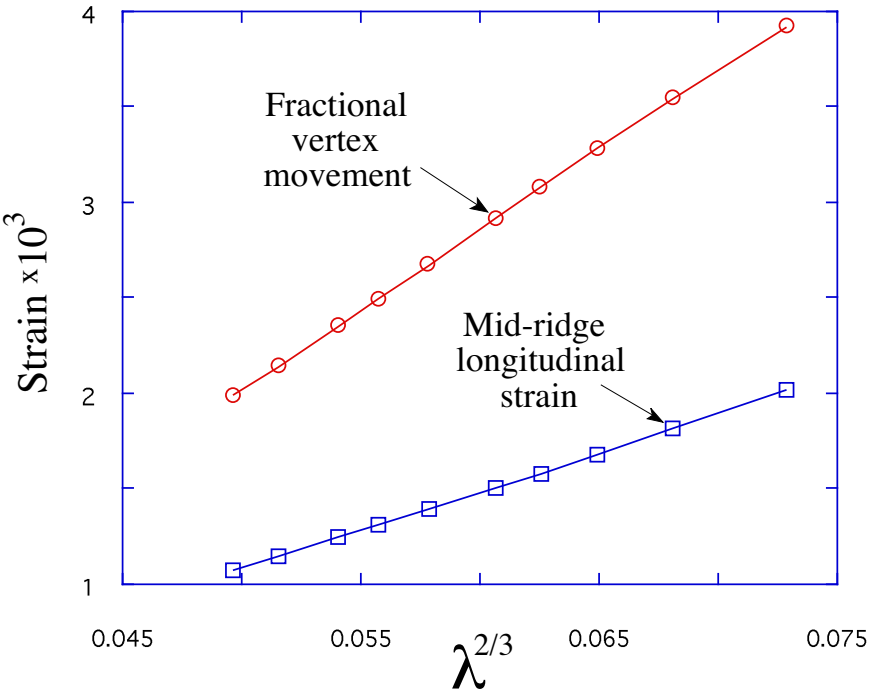

Figure 15. Relative vertex movement divided by X (circles) and the mid-ridge longitudinal strain γ_{xx} (squares) for lattice tetrahedra as a function of the predicted scaling variable $\lambda^{2/3}$. The mid-ridge strain is compressive.

edge of length $50a$ *vs.* the predicted scaling variable $\lambda^{2/3}$. We first note the mid-ridge strain is compressive rather than tensile as the energy scaling argument assumed. The vertices move closer by an amount large enough not only to relieve the extensional strain that would result if the vertices were stationary, but to cause compression along the ridge midline. The strain changes its sign and becomes tensile as one moves away from the ridge midline in the transverse direction.

Another assumption of the energy scaling argument was that the of the ridge sag, *i.e.* the vertical displacement of the middle of the ridge from its limiting straight line shape, is of the order of the ridge radius of curvature. As a consequence, the scaling of the ridge sag with the thickness λ was deduced. In Fig. 16 we plot the ridge

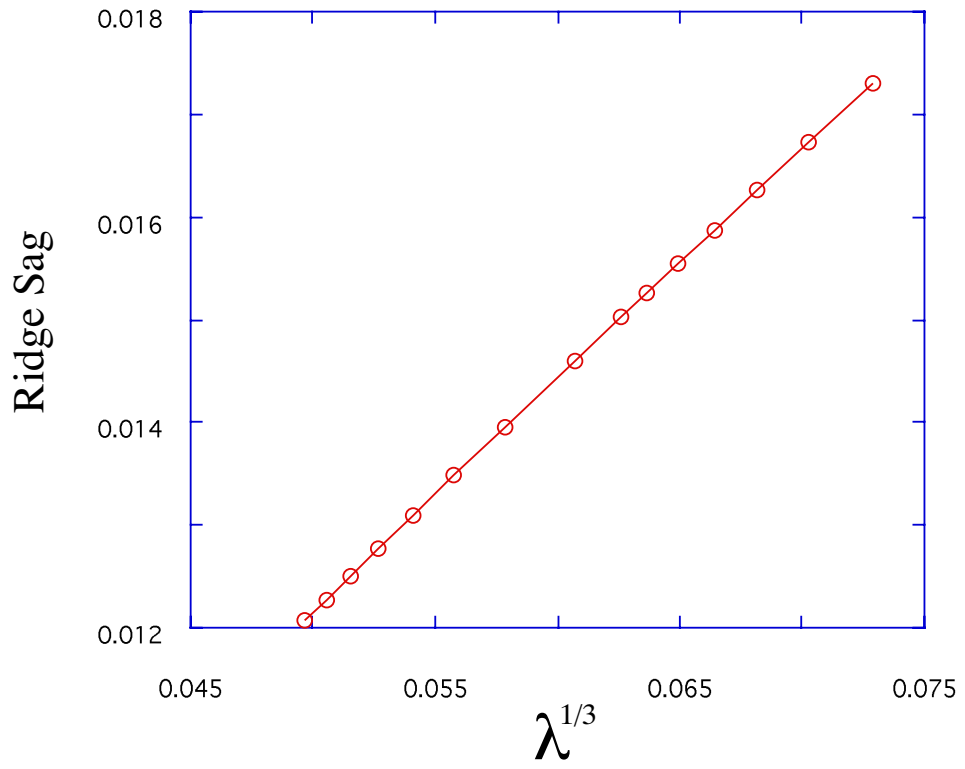

Figure 16. The sagging of the middle of the tetrahedron ridge in units of X as a function of the predicted scaling variable $\lambda^{1/3}$. The straight line fit indicates agreement with the scaling prediction.

sag for a tetrahedron of size $X = 50a$ as a function of the predicted scaling variable $\lambda^{1/3}$. The data fall onto a straight line in agreement with the scaling argument.

The total energy of the tetrahedron is expected to scale as $\kappa(X/h)^{1/3}$. In Fig. 17 we plot the measured total energy of the tetrahedra of sizes $50a$ and $100a$ in units of κ. The energy per ridge is consistent with the asymptotic formula $E = \kappa(1.550 \pm 0.002)(X/h)^{1/3}$. The indicated uncertainty reflects only the scatter in the data used. For comparison, one can show that the combined energy of the four disconnected cones making up the tetrahedron, namely

$$4\kappa(4.081 \log(X/a) + \text{const}), \tag{3.39}$$

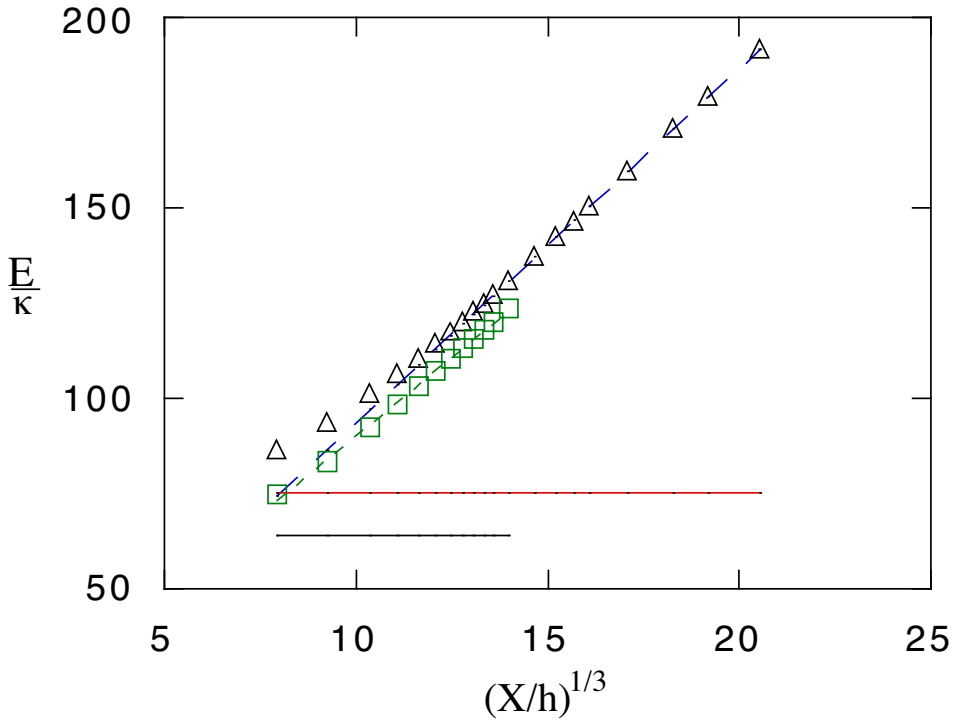

Figure 17. Total elastic energy in the units of the bending modulus κ for lattice tetrahedra with $X = 50$ lattice units (squares) and 100 lattice units (triangles), *vs.* $(X/h)^{1/3} \sim \lambda^{-1/3}$. Dashed lines represent the least-square fits through the upper seven points of the data. Solid lines reflect the energies of four separated cones of length X and sharpness π as in a tetrahedron, using Eq. (3.39) without the additive constant. Lower line: $X = 50$ lattice units; upper line: $X = 100$ lattice units. (Numerically-determined cone energies fall close to these lines.)

is independent of the moduli G and thus independent of the elastic thickness h. The cone energy is purely bending and can be obtained by integrating the squared curvature that is inversely proportional to the distance from the vertex over the area of the cone. The lower limit of integration should be h, but due to the underlying lattice this lower cutoff is really the lattice constant a. Therefore, the cone energy is independent of h in the limit that h is much smaller than the lattice spacing a. In our numerical studies h varied from a to a few percent of a. Accordingly, we observed a few-percent dependence of the cone energy on h. Evidently, the cone energy remains a significant fraction of the tetrahedron energy for all tetrahedra studied. Nevertheless, the asymptotic scaling gives less than ten percent error for tetrahedra larger than about 10^3 times their thickness.

We used the lattice tetrahedra with the edge length of $X = 100a$ to verify another consequence of the energy scaling argument—the virial theorem—that asserted that if all of the elastic energy was concentrated in the ridges then the total bending energy is five times the total bending energy. In Fig. 18 we plot the ratio of the total bending to the total stretching energies as a function of the dimensionless thickness λ. This ratio approaches the predicted value of $E_{\rm bend}/E_{\rm str} = 5$ within a few percent for the values of $\lambda \leq 10^{-4}$. For the smallest values of λ on the plot the ratio deviates from the asymptotic limit due to lattice effects.

We tested the dihedral angle scaling by making a long rectangular strip of dimensions $50a$ by $173a$ and applying normal forces to the perimeter points in such a way that the long boundaries follow a rectilinear frame bent by a dihedral angle $\pi - 2\alpha$. For all angles we fixed the thickness to size ratio $\lambda \simeq 5 \times 10^{-4}$. The results are displayed in Figures 19 and 20. Fig. 19 is a plot of the total elastic energy in units of the bending modulus κ *vs.* the anticipated scaling variable $\alpha^{7/3}$. To a good precision the energy does indeed exhibit the predicted scaling behavior for a wide range of dihedral angles. The deviation at the small bending angles is due to the finite size effects. Since the width of the ridge diverges as $\alpha \to 0$ larger sheets are needed for smaller angles to make sure that the width of the ridge does not exceed the size of

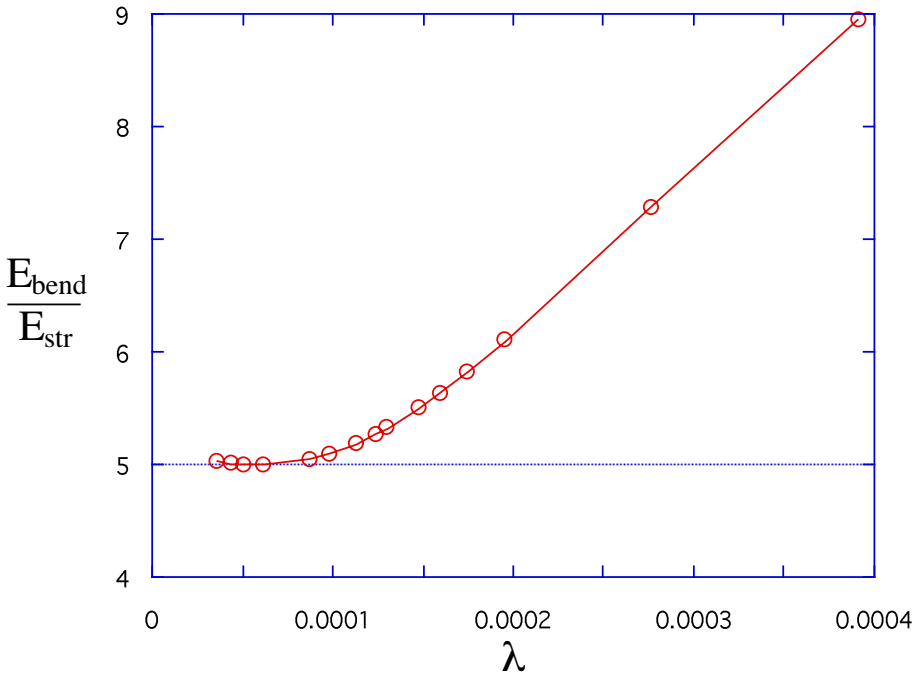

Figure 18. Ratio of the total bending to the total stretching energy *vs.* the dimensionless thickness λ for a regular tetrahedron of edge length $100a$. The predicted asymptotic limit of 5 is approached for $\lambda \simeq 10^{-4}$.

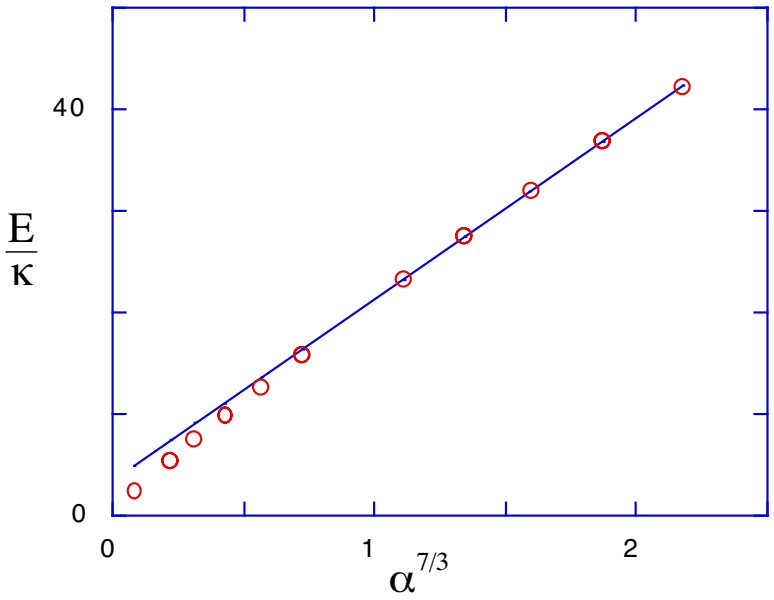

Figure 19. Total elastic energy in units of the bending modulus κ of $50a$ by $173a$ strips of thickness $h = 0.063a$ bent by an angle α. A straight line fit indicates good agreement with the scaling prediction for a large range of dihedral angles.

the sheet used in the simulation. In Fig. 20 the mid-ridge curvature $C_{yy}(0)$ in units of X^{-1} is plotted against $\alpha^{4/3}$. The data agree well with the scaling prediction.

Another test relevant to the question of the boundary condition dependence of the scaling predictions is the comparison of the coefficients R for different boundary conditions in the asymptotic form of the total elastic energy of the ridge $E/\kappa \simeq R\ \lambda^{-1/3}\alpha^{7/3}$. The value of R for the tetrahedral shape, was found by examining the dependence of the energy on λ for a fixed dihedral angle. It was found to be $R_{\rm tet} = 1.161 \pm 0.003$. For the strip geometry we have found $R_{\rm strip} = 1.24 \pm 0.01$ by fixing λ and varying α. Here the error range reflects only the uncertainty arising from scatter in the numerical data. However, there are additional errors resulting from corrections to the asymptotic scaling not properly accounted for in our crude fitting procedure. We therefore suspect that the scaling coefficient R depends insensitively on the boundary conditions and varies only by a fraction of its value. Ref. [44] suggests

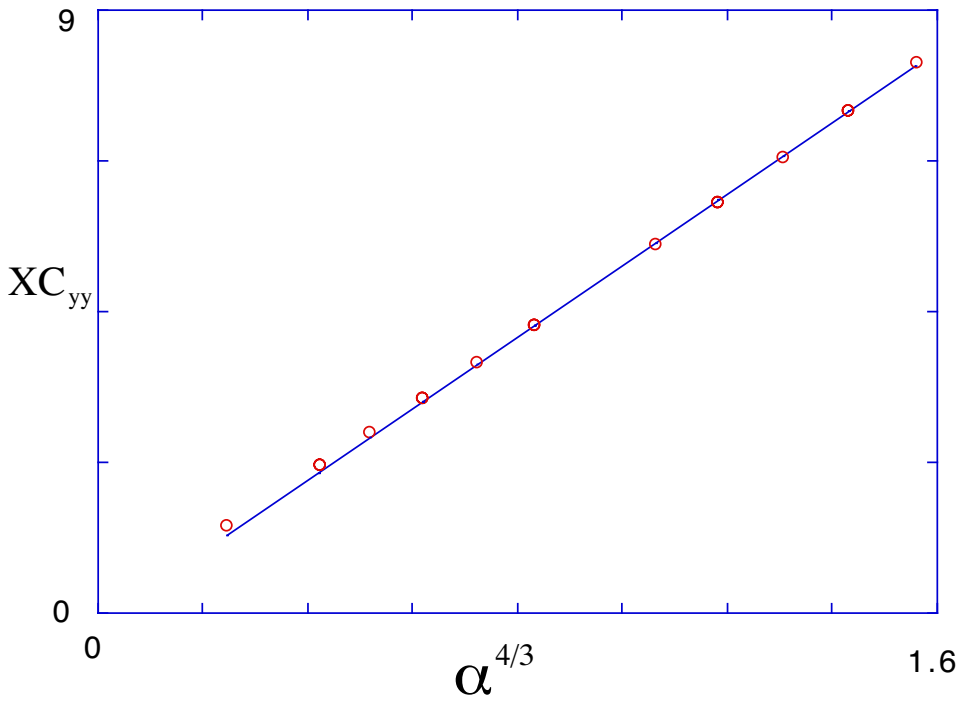

Figure 20. The mid-ridge curvature in units of X^{-1} for the $50a$ by $173a$ bent strips of thickness $h = 0.063a$ *vs.* the anticipated scaling variable $\alpha^{4/3}$.

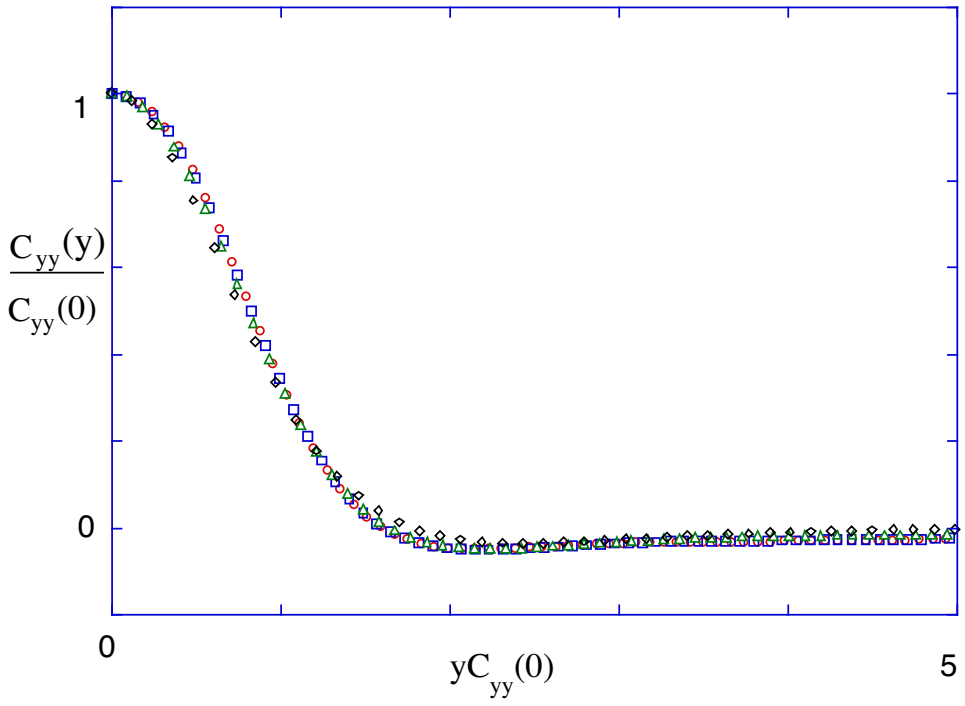

Figure 21. Transverse curvatures $C_{yy}(x,y)$ for $x = 0$ (circles), $x = 5$ (squares), $x = 10$ (triangles) and $x = 15$ (diamonds) each scaled by $C_{yy}(x,0)$ *vs.* the transverse coordinate y scaled by $C_{yy}^{-1}(x,0)$. The curvatures are found numerically from a $50a$ by $433a$ strip bent by a 90 degree angle.

that, in fact, under loading, the energy of a ridge can only change by no more than a finite fraction before the ridge buckles.

A rather suggestive demonstration of the $q(\tilde{x})$-scaling is presented on Fig. 21. We plot the transverse curvatures for different slices $\tilde{x} = const$ obtained from a simulated strip of dimensions $50a$ by $433a$ bent by normal forces applied to the $x = \pm X/2$ parts of the boundary to make a 90 degree angle. The dimensionless thickness is $\lambda \simeq 10^{-3}$. The curvature for each slice is scaled by its value at the origin $\tilde{y} = 0$. The transverse coordinate is scaled by the inverse of the curvature at $\tilde{y} = 0$. These profiles collapse onto a single scaling curve.

Confirmation, beyond just a suggestive illustration, of the $q(\tilde{x})$-scaling of the ridge shape requires more thought since the zeroth order separable solution obtained

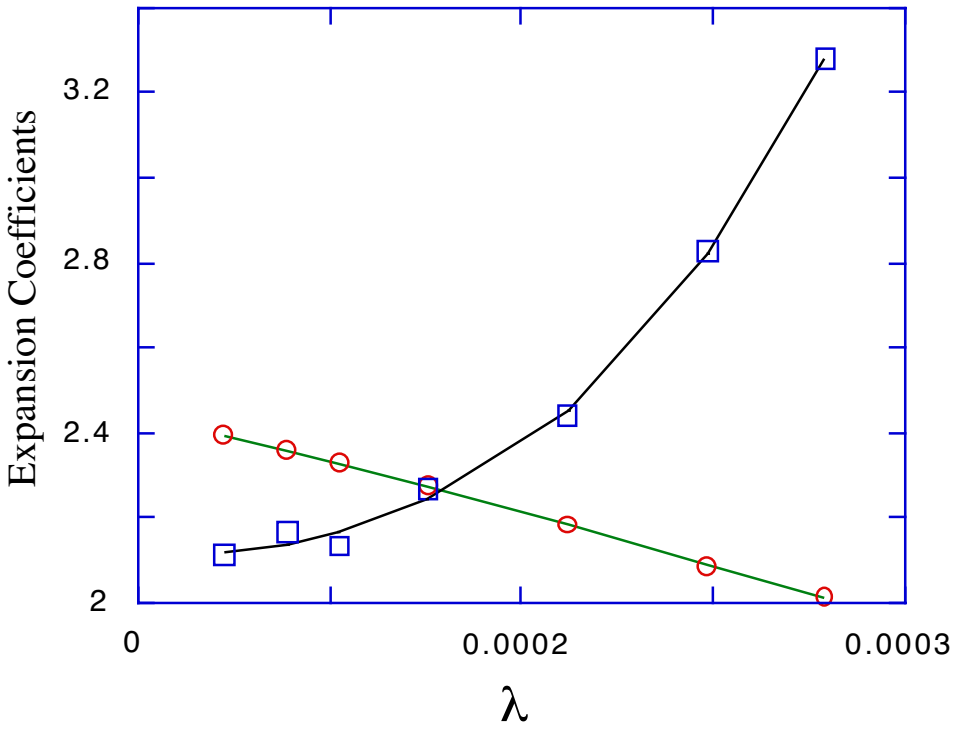

Figure 22. Scale factor expansion coefficients b_2 (circles) and b_4 (squares) as extracted from a least squares fit to the functional form of the transverse radius of curvature along the ridge for tetrahedra of $X = 100a$.

above is only valid in a region around the ridge away from the boundaries. Therefore, to test the predicted functional form of the scale factor $q(\tilde{x})$ one ought to look a *local* property of the numerical solution away from the boundary and find its limit as $\lambda \to 0$. Numerically one has access to only a limited range of thickness to size ratios. (λ cannot be too small otherwise lattice effects become significant.) Nevertheless, the Taylor expansion coefficients of the scale function $q(\tilde{x})$ around $\tilde{x} = 0$ can be successfully extracted from the numerics. Since there is one adjustable parameter $q(0)$ we must look at the first two coefficients in the expansion $q(\tilde{x}) = q(0)(1+b_2\tilde{x}^2+b_4\tilde{x}^4+\ldots)$. Expanding Eq. (3.27) we find that $b_2 = \pi^2/4 \simeq 2.47$ and $b_4 = \pi^4/48 \simeq 2.03$.

For a numerical test we used the longitudinal variation of the transverse ridge radius of curvature that is predicted to be proportional to the scale factor

$R_{yy} = 1/C_{yy} \sim q(\tilde{x})$. The coefficients b_2 and b_4 in the expansion $R_{yy}(\tilde{x}) \simeq R_{yy}(0)(1 + b_2\tilde{x}^2 + b_4\tilde{x}^4)$ can be extracted from the numerics and compared to those obtained from Eq. (3.27). Fig. 22 displays a plot of the coefficients b_2 (circles) and b_4 (squares) versus the dimensionless thickness λ obtained by a least squares quadratic polynomial fit to the functional forms of $R_{yy}(\tilde{x})$ in the range of $|\tilde{x}| \leq 0.2$ for tetrahedra of varying thicknesses but fixed edge length $X = 100a$. We see that these coefficients have a well defined limit as $\lambda \to 0$ which is approached algebraically. The extrapolations to $\lambda = 0$ give $b_2 = 2.53 \pm 0.04$ and $b_4 = 2.09 \pm 0.07$ as compared to the predicted values of $b_2 \simeq 2.47$ and $b_4 \simeq 2.03$.

3.5. Conclusions and Unsolved Problems

We examined a straight ridge singularity in bending of thin elastic plates. These singularities are thought to arise under quite general circumstances. The details of how the sharp crease singular limit is approached were established. We found that certain ridge properties asymptotically depend only on a few geometric characteristics of the ridge. These properties were found by an energy scaling argument the essence of which is that ridge behavior is governed by a competition of the bending and the stretching energies that vary as a power of the characteristic ridge curvature. A boundary layer analysis of the von Kármán plate equations puts the conclusions of the energy scaling argument on a firmer footing. We note that the equations used to describe the elastic sheet assumed linear stress-strain relations. Since the strains in the ridge were found to vanish in the limit of small thickness, the results should be applicable to the real materials in which the linear stress-strain relations are more accurate at small strains. We find that boundary layer solution exhibits three types of scaling (or self-similar structure) in the singular limit $\lambda \to 0$.

The λ-scaling seems to be inevitable and depends only on the geometry of the singularity. The asymptotic λ-scaling laws for the characteristic ridge curvature, the ridge strain, the ridge width, the ridge sag, and the elastic energy were established. The elastic energy consists of comparable amounts of the bending and the stretching

energies. A virial theorem that relates the bending and stretching contributions to the total elastic energy has been derived from an energy scaling argument and verified numerically. The virial theorem affords a useful test of elastic energy confinement. When most of the elastic energy is confined to the ridges the virial theorem predicts $E_{\rm bend}/E_{\rm str} = 5$ for the ratio of the bending and the stretching energies in the limit of the vanishing thickness.

The ridge λ-scaling is by no means a unique type of scaling. Scheidl and Troger [38] found that a ring ridge that appears in strong axisymmetric buckling of a spherical shell has a width that scales as $\lambda^{1/2}$ as opposed to the $\lambda^{1/3}$ scaling for the width of the straight ridge singularity examined in this article. The property that makes the straight ridge important is that its energy grows slower with size than that of the ring ridge. The ring ridge is therefore unstable to breakup into straight ridges when the cost of distorting the rest of the sphere can be overcome by the energy gain from the formation of the straight ridges. This point is illustrated in Fig. 23. A cone that has been poked through to create a ring ridge, spontaneously breaks up into three straight ridges. We believe that straight ridges are the dominant type of the singularity in crumpled thin elastic sheets. The morphology of a crumpled sheet can thus be represented as a network of straight ridges that bound flat facets. Since in the thin limit the elastic energy is concentrated into a progressively smaller fraction of the crumpled sheet, the ridges can, at least in the first approximation, be treated as independent. Therefore, once the ridge network is given characterization in terms of the distribution of the lengths and the dihedral angles of the ridges, the elastic energy of the crumpled sheet is given by the sum $E/\kappa \simeq \sum_i R_i \lambda_i^{-1/3} \alpha_i^{7/3}$. The scaling coefficients R_i depend on the details of the boundary conditions such as the external load supported by each ridge. Preliminary studies show [44] that R_i varies at most by a finite fraction.

The second type of scaling is the dihedral angle scaling of the ridge properties. A small angle argument that made an assumption about the transverse ridge shape predicted the scaling of the total energy, the ridge curvature and other quantities with the angle. Analysis of the the separable solution of the rescaled von Kármán

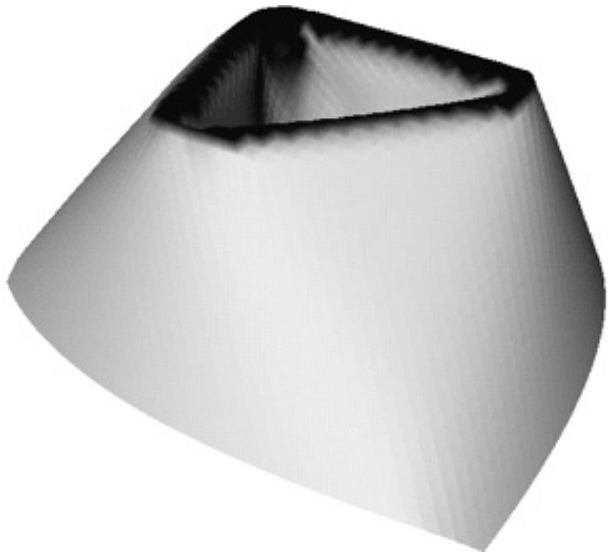

Figure 23. A cone with the vertex of sharpness π(integrated Gaussian curvature) has been poke through with the purpose of creating a ring ridge of the type discussed by Scheidl and Troger. Instead, the ring ridge broke up into three straight ridges.

equations show that the dihedral angle scaling behavior persists up to arbitrary dihedral angles α. This type of scaling only depended on the *form* of the transverse equations and not on the nature of their solution and thus is likely to be independent of the details of the boundary conditions.

The third type of scaling exhibited by the ridge in the small thickness limit is the self-similarity of the ridge shape. By assuming the $q(\tilde{x})$-scaling we are led to a separable dependence on the longitudinal and transverse position. Neither the scaling nor the separability, however, have been proven. We have only found suggestive numerical evidence supporting separability by examining different slices of the ridge. In addition, the first two coefficients in the Taylor expansion of the scale factor $q(\tilde{x})$ have been found to agree with the numerics. A more rigorous test of separability is still needed. The transverse profile of the ridge is most likely dependent on the boundary conditions since the transverse equations contain non-universal integration constants. In fact, the transverse curvature oscillations away from the ridge in the tetrahedron shape is different from that in the strip shape. The simplicity of the

transverse equations also needs to be better understood. Usually such simplicity reflects some underlying physical symmetry in the problem.

A future program aimed at a successful description of forced crumpling must include first, a rigorous proof of the straight ridge morphology of the crumpled state. This amounts to showing that if the size of the sheet and the compression factor are kept fixed there is a well-defined limit for the shape in the limit of the vanishing thickness that is a network of straight ridges that bound flat facets. Second, an understanding of the "non-universal" ridge properties, such as the coefficient in the energy scaling, for example, that depend on the details of the boundary conditions, is needed. These details include external loads that must be applied to collapse the sheet in the first place. In particular, the way in which these external loads are distributed through the crumpled membrane must be understood. Other ridges in the network also modify the boundary conditions for a given ridge leading to a ridge interaction. Third, since further compactification of a crumpled sheet proceeds by a proliferation of the ridges via buckling, one must establish the buckling threshold and the buckling modes of a ridge. Fourth, the self-avoidance constraints must be included in the study of the forces that cause the ridges to buckle.

The main question to be addressed is whether, in fact, a specification of the ridges in terms of their lengths and dihedral angles is sufficient to estimate the elastic energy of a crumpled membrane The answer hinges on a study of the ridge buckling properties. Preliminary results [44] suggest that the elastic energy of a ridge can change due to external influences by at most a finite fraction before it buckles. A comprehensive model of the crumpling dynamics would have to incorporate all of the aspects of the ridge behavior mentioned above.

REFERENCES

[1] P. Stutenkemper and R. Brasche, in *Seventh International Technical Conference on Experimental Safety Vehicles* (US Dept. of Transportation, Washington, DC, 1979).

[2] in *Shock and Vibration Handbook*, edited by C. M. Harris and C. E. Crede (McGraw-Hill, New York, NY, 1988), Chap. 31,41.

[3] K. Svoboda, C. F. Schmidt, D. Branton, and S. M. Block, Biophysical Journal **63**, 784 (1992).

[4] E. Sackmann *et al.*, Ber. Bunsenges. Phys. Chem. **89**, 1198 (1985).

[5] R. H. Mueller, W. Mehnert, J.-S. Lucks, and C. Schwarz, European Journal of Pharmaceutics and Biopharmaceutics **41**, 62 (1995).

[6] R. R. Chianelli, E. B. Prestrige, T. A. Pecoraro, and J. P. DeNeufville, Science **203**, 1105 (1979).

[7] M. S. Spector, E. Naranjo, and J. A. Zasadzinski, Phys. Rev. Lett. **73**, 2867 (1994).

[8] *Statistical Mechanics of Membranes and Surfaces*, edited by D. Nelson, T. Piran, and S. Weinberg (World Scientific, Singapore, 1989).

[9] N. Yamaki, *Elasic Stability of Circular Cylindrical Shells* (Horth-Holland, New York, NY, 1984).

[10] J.-M. Park and T. C. Lubensky, Phys. Rev. E **53**, 2648 (1996).

[11] H. S. Seung and D. R. Nelson, Phys. Rev. A **38**, 1005 (1988).

[12] in *A Treatise on the Mathematical Theory of Elasticity*, fourth ed., edited by A. E. H. Love (University Press, Cambridge, 1927), pp. 29,459.

[13] H. Reissner, in *Spannugen in Kugelschalen-(Kuppeln)* (Mueller-Breslau, Leipzig, 1912), p. 181.

[14] D. G. Ashwell, Proc. Roy. Soc. A **214**, 98 (1952).

[15] J. J. O'Dwyer, *The Theory of Dielectric Breakdown of Solids*, *Monographs on the Physics and Chemistry of Materials* (Clarendon Press, Oxford, 1964).

[16] A. A. Griffith, Phil. Trans. Roy. Soc. Lond. **A221**, 163 (1920).

[17] R. J. Gaylord and J. F. Douglas, Polym. Bull. **18**, 347 (1987).

[18] J. Washiyama, E. J. Kramer, , and C.-Y. Hui, Macromolucules **28**, 1654 (1995).

[19] M. Tinkham, *Introduction to Superconductivity* (McGraw-Hill, New York, 1975).

[20] M. C. Cross and P. C. Hohenberg, Rev. Mod. Phys. **65**, 2 (1993).

[21] L. Prandtl, *Essentials of Fluid Dynamics* (Blackie & Son Limited, London, 1952).

[22] in *International Conference on Grain Growth in Polycrystalline Materials (Rome, Italy)* (Trans Tech Publications, Zurich, Switzerland, 1992).

[23] J. M. Calderon-Moreno, A. D.-R. A. R. De Arellano-Lopez, and J. L. Routbort, Journal of the European Ceramic Society **15**, 983 (1995).

[24] C. h. Liu *et al.*, Science **269**, 513 (1995).

[25] in *Confinement 95: International RCNP Workshop on Colour Confinement and Hadrons, RCNP Osaka, Japan*, edited by H. Toki (World Scientific, Singapore, New Jersey, 1995).

[26] M. B. Green, *Superstring Theory*, *Cambridge Monographs on Mathematical Physics* (Cambridge University Press, Cambridge, New York, 1987).

[27] A. Föppl, *Vorlesungen über Technische Mechanik* (B. G. Turner, Leipzig, Berlin, 1907), Vol. 5.

[28] T. von Kármán, *Collected Works* (Butterworths, London, 1956).

[29] F. John, Comm. Pure. Appl. Math. **18**, 235 (1965).

[30] W. T. Koiter, Proc. Kon. Nederl. Acad. Wet. Amsterdam **B69**, 1 (1966).

[31] P. G. Ciarlet, Arch. Rat. Mech. Anal. **73**, 349 (1980).

[32] E. H. Mansfield, *The Bending and Stretching of Plates* (Pergamon, New York, 1984).

[33] G. H. Knightly and D. Sather, Arch. Rat. Mech. Anal. **72**, 315 (1980).

[34] L. D. Landau and E. M. Lifshitz, in *Theory of Elasticity* (Pergamon, Oxford, 1986), Chap. 14,15.

[35] R. S. Milman and G. D. Parker, *Elements of Differential Geometry* (Prentice Hall, Inc., Englewood Cliffs, New Jersey, 1977).

[36] A. E. Green, Proc. Roy. Soc. Ser. A **269**, 481 (1962).

[37] Y. C. Fung and W. H. Wittrick, Quart. J. Mech. Appl. Math. **VIII**, 191 (1955).

[38] R. Scheidl and H. Troger, Computers and Structures **27**, 157 (1987).

[39] E. M. Kramer, Ph.D. thesis, The University of Chicago, 1996.

[40] M. B. Amar and Y. Pomeau, La Recherche **26**, 45 (1995).

[41] A. E. Lobkovsky *et al.*, Science **270**, 1482 (1995).

[42] T. A. Witten and H. Li, Europhysics Letters **23**, 51 (1993).

[43] J. Mathews and R. L. Walker, *Mathematical Methods of Physics* (Addison-Wesley, Reading, Mass, 1970).

[44] A. E. Lobkovsky and T. A. Witten, to be submitted to Phys. Rev. E (unpublished).